Catecholamines, not acetylcholine, alter cortical and perceptual dynamics in line with increased excitation-inhibition ratio

Thomas Pfeffer (1), Arthur-Ervin Avramiea (2), Guido Nolte (1), Andreas K. Engel (1), Klaus Linkenkaer-Hansen (2), Tobias H. Donner (1,3,4)

1 Department of Neurophysiology and Pathophysiology, University Medical Center Hamburg-Eppendorf, Hamburg, Germany
2 Center for Neurogenomics and Cognitive Research, Neuroscience Campus Amsterdam, VU University Amsterdam, The Netherlands
3 Department of Psychology, University of Amsterdam, The Netherlands
4 Amsterdam Brain and Cognition, University of Amsterdam, The Netherlands

Correspondence:
thms.pfffr@gmail.com (T.P.)
t.donner@uke.de (T.H.D.)

Abbreviated title: Neuromodulation and Cortical Excitation-Inhibition Balance

ABSTRACT

The ratio between excitatory and inhibitory neurons (E/I ratio) is vital for cortical circuit dynamics, computation, and behavior. This ratio may be under the dynamic control of neuromodulatory systems, which are in turn implicated in several neuropsychiatric disorders. In particular, the catecholaminergic (dopaminergic and noradrenergic) and cholinergic systems have highly specific effects on excitatory and inhibitory cortical neurons, which might translate into changes in the local net E/I ratio. Here, we assessed and compared their net effects on net E/I ratio in human cortex, through an integrated application of computational modeling, placebo-controlled pharmacological intervention, magnetoencephalographic recordings of cortical activity dynamics, and perceptual psychophysics. We found that catecholamines, but not acetylcholine, altered both the temporal structure of intrinsic activity fluctuations in visual and parietal cortex, and the volatility of perceptual inference based on ambiguous visual input. Both effects indicate that catecholamines increase the net E/I ratio in visual and parietal cortex.

INTRODUCTION

Cortical activity fluctuates continuously, even in the absence of changes in sensory input or motor output (1). These intrinsic fluctuations in cortical activity are evident from the level of single neurons to large-scale networks of distant cortical areas (2–4). Fluctuations in cortical mass activity, specifically the amplitude modulation of ongoing oscillations, exhibit temporal structure characteristic of so-called “scale-free” behavior: Power spectra that scale as a function of frequency according to a power law, $P(f) \propto f^{\beta}$ (5,6), and long-range temporal autocorrelations (7–10). This temporal structure of cortical activity varies widely across individuals, is partly explained by genetics (11), and it exhibits marked changes in brain disorders (12,13).

The large variability of cortical activity is not only due to the biophysics of individual cells (1), but also due to the balance between excitatory and inhibitory inputs to each neuron (2,14). The ratio between excitatory and inhibitory interactions in local cortical circuits, henceforth referred to as E/I ratio, is also essential for the characteristic structure of spontaneous cortical activity (15,16). For example, structural variations of excitatory and inhibitory connectivity affect the temporal structure of activity fluctuations in a model of a local cortical circuit (15). Finally, the E/I ratio is also a key determinant of the computational properties of individual cortical neurons (17,18) as well as the behavior of the organism, as shown for perceptual categorization tasks (16,18–21).

This key property of cortical circuits, E/I ratio, might not be a fixed property of cortex, but rather under dynamic control. One factor in particular might be key for regulating cortical E/I ration and thus cortical variability as well as behavior: dynamic variations in neuromodulatory tone (22). Modulatory systems of the brainstem regulate cortical state through widespread ascending

projections, and they are implicated in most of the major neuropsychiatric disorders (17,23–26). The modulatory neurotransmitters released from these systems, such as noradrenaline or acetylcholine, alter specific elements (pyramidal cells or inhibitory interneurons) of cortical microcircuits (27,28) as well as the variability of cortical neurons (27,29,30). Critically, whether and how neuromodulatory systems change the net E/I ratio and ongoing activity fluctuations within local populations of cortical neurons has remained unknown. A systematic, empirical assessment of the net effects on cortical E/I ratio in human cortex would be key for understanding how synaptic and cellular effects of neuromodulation translate into changes in human cognition and behavior, as well as into disturbances thereof in brain disorders. However, inferences on cortical net E/I ratio based on standard “resting-state” measurements of human cortical population activity have, so far, been challenging.

Here, we aimed to overcome this challenge through the integrated application of computational modeling, magnetoencephalographic (MEG) recordings of fluctuations in cortical population activity under different pharmacological interventions and “steady-state” task conditions, and psychophysical measurements of bistable perceptual dynamics that are sensitive to cortical E/I ratio (21,31,32). This integrative approach enabled us to systematically image and compare the effects on the cortical net E/I ratio of two major groups of neuromodulatory systems: the catecholaminergic (noradrenergic and dopaminergic) and cholinergic systems. Importantly, we read out their effects on cortical net E/I ratio from two separate measurements: changes in the intrinsic fluctuations in cortical activity and of bistable perceptual dynamics. Both yielded convergent evidence for an increase of net E/I ratio in visual and parietal cortex due to catecholamines, but not acetylcholine.

RESULTS

We tested for changes in intrinsic perceptual and cortical dynamics under placebo-controlled pharmacological manipulations of catecholamine (using atomoxetine) and acetylcholine (using donepezil) levels (Fig 1A). Importantly, intrinsic fluctuations in cortical activity were measured during two steady-state conditions (Fig 1B): (i) fixation of an otherwise gray screen (Fixation), as in most common studies of human "resting-state" activity; and (ii) silent counting of the spontaneous perceptual alternations induced by a continuously presented, ambiguous visual stimulus (Task-counting). In a third condition, subjects immediately reported the perceptual alternations by button-press (Task-pressing).

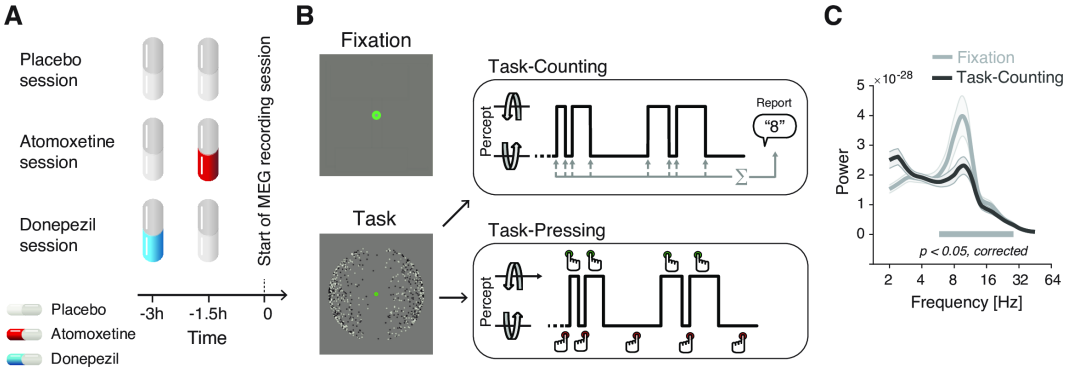

Fig 1. Experimental design **(A, B)** Types and time course of experimental sessions. **(A)** Each subject participated in three sessions, involving administration of placebo, atomoxetine, or donepezil (session order randomized across subjects). Each session entailed the administration of two pills, in the order depicted for the different session types. **(B)** Within each session, subjects alternated between three conditions, Fixation, Task-Counting and Task-Pressing, during which MEG was recorded (runs of 10 min each). See Materials and Methods for details. **(C)** Group average power spectrum, averaged across all MEG sensors, for Rest and Task (Placebo condition only).

This design capitalized on recent insights into the changes in cortical E/I-ratio under sensory stimulation (33,34) and on the effects of cortical E/I-ratio on bistable perceptual dynamics (21,31,32). These previous insights and our experimental data combined, allowed for interpreting the latter in terms alterations in net cortical E/I ratio under the pharmacological treatments.

To solidify our predictions about the impact on modulations of E/I ratio on the intrinsic correlation structure of cortical population activity, we also simulated the population activity of a simplified cortical circuit model made up of recurrently connected excitatory and inhibitory neurons, under systematic variations of gain modulation at different synapse types.

The Results section is organized as follows. We first present the effects of the drugs on perceptual alternation rate. We then show how dynamic variations of E/I ratio due to synaptic gain modulation alter intrinsic fluctuations in the amplitude of cortical oscillations of a cortical circuit model. Next, we show how manipulating catecholaminergic and cholinergic neuromodulation, affects fluctuations in cortical activity—specifically, the temporal correlation structure of intrinsic fluctuations in the amplitude of cortical oscillations (Fig 2), during both steady-state conditions (Fixation and Task-counting). Finally, we discuss the drug effects on other measures of cortical activity as well as peripheral signals. These controls support the validity and specificity of our main conclusions.

Atomoxetine increases the rate of perceptual alternations compared to placebo and donepezil

We used the rate of the reported alternations in perception of the ambiguous visual structure-from-motion stimulus (Fig 1B) as a behavioral proxy for changes in cortical E/I ratio in visual cortex. Current models of the neural dynamics underlying bistable perception postulate that such perceptual alternations emerge from the interplay between feedforward drive of stimulus-selective neural populations in sensory cortex, mutual inhibition between them, adaptation, and noise (31,32). Convergent evidence from model simulations (21) as well as functional magnetic resonance imaging, magnetic resonance spectroscopy, and

pharmacological manipulation of GABAergic transmission (21,35) indicates that increases in the ratio between feedforward, excitatory input to, and mutual inhibition within the cortical circuit give rise to faster perceptual alternation rates.

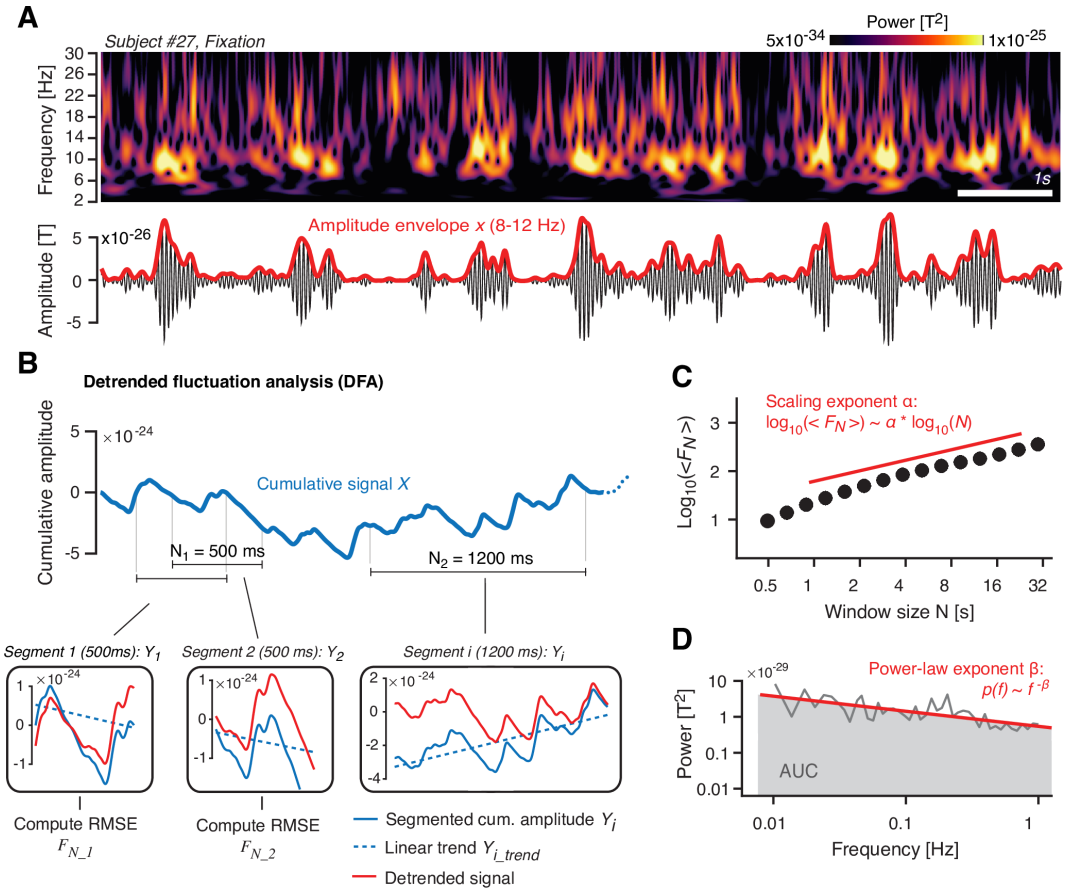

Fig 2. Quantifying the temporal structure of fluctuations in oscillatory cortical activity
(A) *Top.* Time-frequency representation of MEG power fluctuations during Rest (example subject). *Bottom.* Filtered signal (10 Hz; black) and the corresponding amplitude envelope (red). **(B)** Illustration of detrended fluctuation analysis. See main text (Materials and Methods) for details. *Top.* Cumulative sum of the amplitude envelope. *Bottom.* Detrending of cumulative sum within segments, shown for two different window lengths *N* (N_1 = 500 ms and N_2 = 1200 ms). **(C)** Root-mean-square fluctuation function $<F_N>$. In log-log coordinates, $<F_N>$ increases approximately linearly as a function of *N*, with a slope that is the scaling exponent α. **(D)** Illustration of power spectrum analysis of amplitude envelope. In log-log coordinates, the power spectrum can be approximated by a straight line, with a slope β (power-law exponent) and an area under the curve (gray) that quantifies the overall variance of the signal.

In this study, atomoxetine increased the rate of perceptual alternations compared to both, placebo and donepezil (Fig 3A; atomoxetine vs. placebo: p = 0.007; t = 2.913; atomoxetine vs. donepezil: p = 0.001; t = 3.632; donepezil vs. placebo: p = 0.966; t = -0.043; all paired t-tests, pooled across Task-counting and Task-

pressing). This atomoxetine effect on the perceptual dynamics was also significant for Task-counting (p = 0.045; t = 2.103; paired t-test; Fig S1A) and Task-pressing (p = 0.018; t = 2.540; paired t-test; Fig S1B) individually, and the perceptual alternation rates were highly consistent across both conditions (Fig S1C).

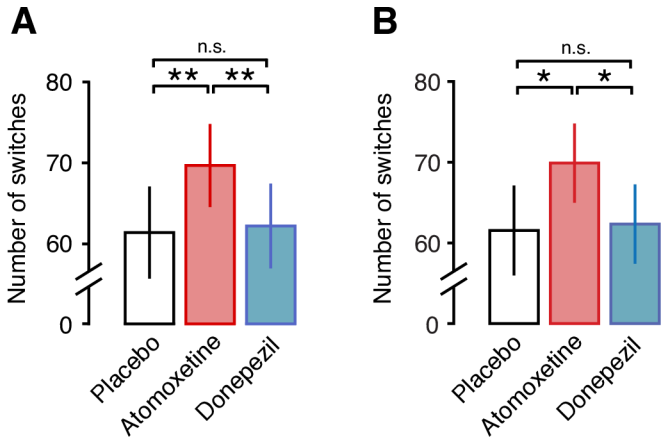

Fig 3. Atomoxetine, but not donepezil, increases the rate of perceptual alternations **(A)** Number of perceptual alternations reported by the subjects per 10 min run, pooled across task conditions (Task-counting and Task-pressing). **(B)** Same as (A), after removing blink and eye movement data (with linear regression).

One potential concern is that atomoxetine might have increased the rates of spontaneous eye blinks or fixational eye movements, inducing retinal transients and thus fluctuations in visual cortical activity and perception, without any change in intra-cortical E/I ratio. Three observations rule out this concern. First, there was no significant increase during atomoxetine compared to placebo in any of five different eye movement parameters measured here (Fig S2). Second, none of the eye movement parameters correlated significantly with the perceptual alternation rate (Fig S2). Third, and most importantly, the effect of atomoxetine on the perceptual dynamics was also significant after removing (via linear regression) the individual eye movement parameters (Fig 3B).

In sum, the psychophysical results are consistent with an atomoxetine-induced increase in the net E/I ratio. This change should have occurred in cortical

208 circuits within the dorsal visual stream that govern the perceptual dynamics of
209 ambiguous structure-from-motion signals (36).
210
211 **Effects of synaptic gain modulation on scaling behavior in a cortical circuit**
212 **model**
213 We used the temporal correlation structure of fluctuations in cortical activity as a
214 separate read-out of changes on cortical E/I ratio, guided by simulations of
215 cortical circuit models under neuromodulation. The models of bistable perception
216 discussed above are sufficient for generating perceptual time courses, but are not
217 sufficiently realistic to generate the features of cortical mass activity evident in
218 physiological recordings of local field potentials or MEG signals (e.g., alpha-band
219 oscillations, scale-free amplitude envelope fluctuations). We used a more
220 complex cortical circuit model that does exhibit these features (15) as a starting
221 point for our modeling work (Fig 4). The model has previously been used to show
222 that scale-free intrinsic fluctuations in cortical activity are highly sensitive to
223 variations in the structural E/I ratio (i.e., the percentage of excitatory and
224 inhibitory connections) in the circuit (15). This model accounts for the joint
225 emergence of two empirically established scale-free behaviors, which we
226 reproduced: (i) neuronal avalanches, activity patterns propagating through the
227 network as evident in recordings from microelectrode arrays, with an event size
228 distribution following a power-law (37); and (ii) long-range temporal correlations
229 of the amplitude envelope fluctuations of the model's local field potential, which
230 we assessed empirically through MEG recordings. The power-law scaling of
231 avalanche size distribution was quantified in terms of the kappa-index, which
232 quantifies the similarity between the measured avalanche size distribution and a

theoretical power-law distribution with an exponent of -1.5 (38); a kappa index of 1 indicates perfect match between the two.

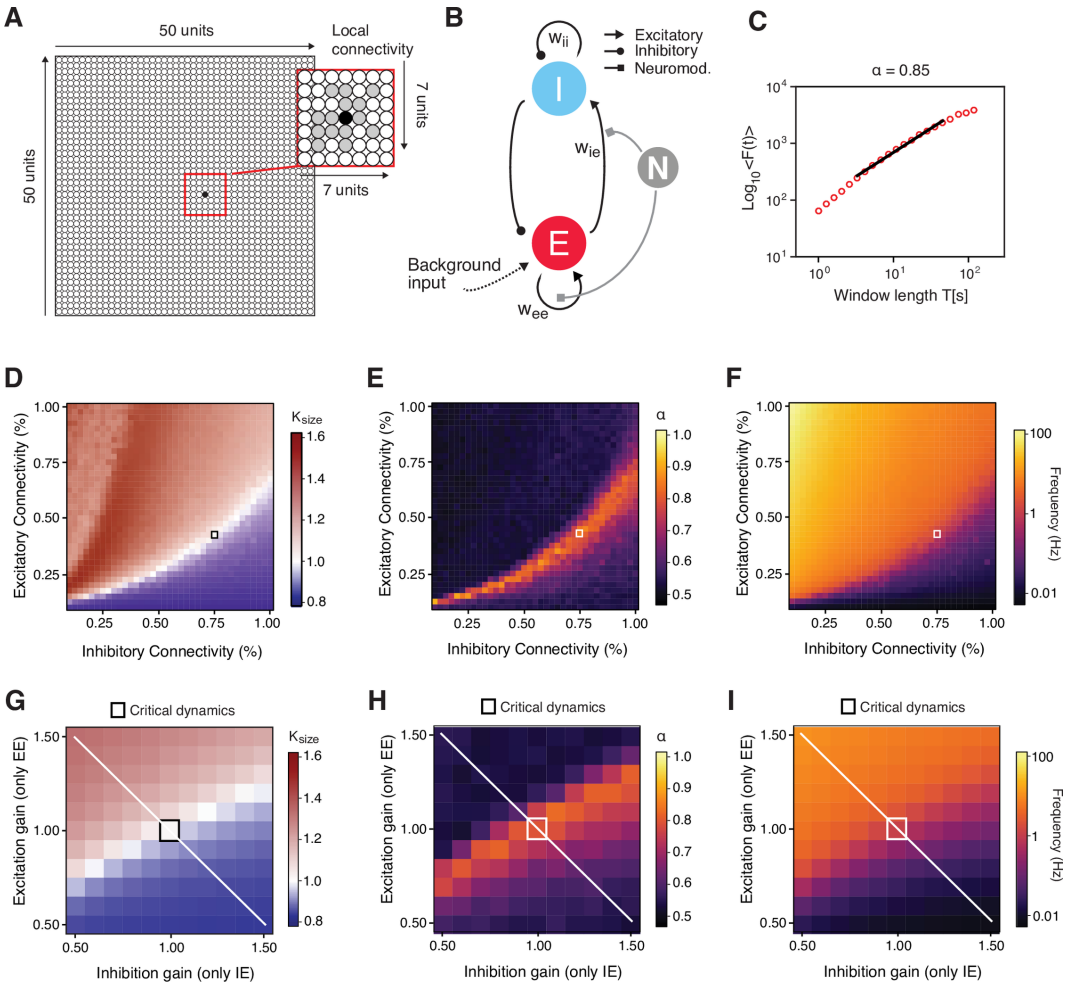

Fig 4. Dynamic modulation of excitation-inhibition ratio alters long-range temporal correlations in model of cortical patch. **(A)** Schematic of the computational model. The network consisted of 2500 excitatory and inhibitory integrate-and-fire units and random, local (within an area of 7x7 units) connectivity (magnified within the red square). **(B)** Neuromodulation was simulated as a gain modulation term multiplied with excitatory synaptic weights (w_{ee} and w_{ie}). **(C)** Detrended fluctuation analysis of model simulation (scaling exponent α of 0.85). **(D)** κ as a function of excitatory and inhibitory connectivity (with a spacing of 2.5%; means across 10 simulations per cell). The region of κ~1, overlaps with the region of $\alpha > 0.5$ and splits the phase space into an excitation-dominant (κ>1) and an inhibition-dominant region (κ<1). The black square depicts the network configuration that was chosen for assessing the effects of neuromodulation **(E)** Scaling exponent α as a function of excitatory and inhibitory connectivity. **(F)** Same as (D) and (E), but for mean firing rate. **(F)** κ as a function of independent synaptic gain modulation. **(G)** Same as (D), but for scaling exponent α. **(H)** Same as (G), but for firing rate. Red square, baseline state of critical network before neuromodulation was applied. White line, axis of parameter combinations corresponding to changes in excitation-inhibition ratio re-plotted schematically in Fig 8.

The two phenomena unfold on different scales of spatial resolution (single neurons vs. mass activity summed across neurons) and different temporal scales (tens of milliseconds vs. several hundred seconds). Yet, both phenomena have

been found to emerge at the same ratio between structural excitatory and inhibitory connectivity (15), and we replicated this finding here (Fig 4D-F).

Critically, we extended this model with a modulatory mechanism in order to assess the impact of dynamic, multiplicative changes in cortical E/I ratio that might result from catecholamines or acetylcholine. We first determined the structural connectivity (small squares in Fig 4D-F) and the time scale parameters such that the network generated intrinsic alpha-band oscillations with amplitude fluctuations that exhibited robust long-range temporal correlations (with $\alpha \sim 0.85$, Fig 4C), as well as neuronal avalanches with scale-free size distributions (Materials and Methods). We then independently modulated synaptic connections through multiplicative scaling of the weights (as illustrated in Fig 4B).

Two separate versions of the synaptic gain modulation yielded qualitatively similar effects. In the first version shown in Fig 4, we modulated only excitatory synapses, but independently on excitatory as well as inhibitory neurons (EE and IE), thus producing asymmetries in the circuits net E/I ratio as in recent modeling work on the effects of E/I ratio on a cortical circuit for perceptual decision-making (18). In the second version (Fig S3A), we co-modulated EE and IE and independently modulated inhibitory synapses on excitatory neurons (EI). This was intended to simulate modulations of the GABA receptors in the former case (mediating the effects of inhibitory neurons on others), as opposed (AMPA or NMDA) glutamate receptors in both of the latter two cases (mediating the effects of excitatory neurons on others). N_{EE} and N_{IE} were co-modulated by the same factor for simplicity, because we did not assume that excitatory (glutamatergic) synapses would be differentially modulated depending on whether they were situated on excitatory or inhibitory target neurons.

In both versions of the model, changes in net E/I ratio altered κ (Fig 4G and Fig S3B) as well as the scaling exponent α (Fig 4H and Fig S3C) and mean firing rate (Fig 4I and Fig S3D). Importantly, the effect of changes in E/I ratio on the scaling exponent α were non-monotonic, dependent on the starting point: increases in excitation led to increases in α when starting from an inhibition-dominant point, but to decreases in α when starting from an excitation-dominant point (Fig 4G-I, white line).

The effects of excitatory and inhibitory gain modulation on the temporal correlation structure of the simulated activity were qualitatively similar to the effects of (structural) changes in the fraction of excitatory and inhibitory synapses simulated (as shown in Fig 4D-F). We conceptualize the latter as simulations of individual differences in cortical anatomical microstructure, and the former as simulations of within-subject, state-dependent changes in cortical dynamics, which are the focus of the current study. The new simulation results provided a solid foundation for the interpretation of the pharmacological effects on fluctuations of alpha-band amplitude envelope signals in human MEG data, described next.

Atomoxetine, not donepezil, increases the scaling exponent of cortical activity

We found a subtle, but robust and highly consistent increase in the scaling exponent α of fluctuations in human MEG under atomoxetine, but not donepezil (Fig 5 and Fig 6). We focused our analyses on amplitude envelope fluctuations in the 8–12 Hz frequency range (“alpha band”), for two reasons. First, as expected from previous work (39), the cortical power spectra exhibited a clearly discernible in this frequency range, which robustly modulated with task conditions

306 (suppressed under Task-counting, Fig 1C). Second, the parameters of the above
307 model were tuned to produce oscillations in the same range (see above and (15)).

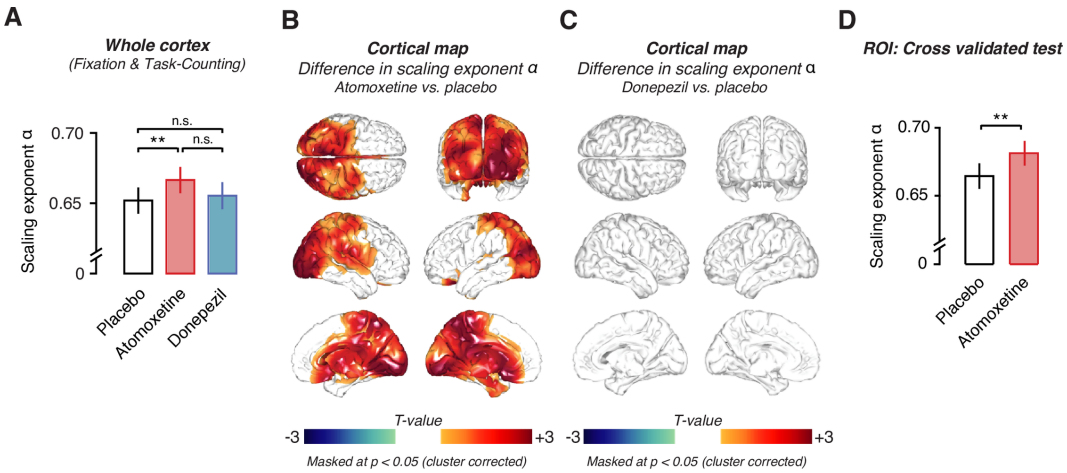

308
309
310 **Fig 5.** Scaling exponent α for the pharmacological conditions, pooled across Fixation and Task-
311 counting conditions. **(A)** Mean scaling exponent across all voxels (N = 3000) for all three
312 pharmacological conditions. Compared to placebo, the exponent exhibits a significant increase
313 under atomoxetine, but not under donepezil. **(B, C)** Spatial distributions of drug-induced changes
314 (threshold: at p = 0.05, two-sided cluster-based permutation test). **(B)** atomoxetine vs. placebo; **(C)**
315 donepezil vs. placebo. **(D)** Cross-validation approach, see Results for details.
316
317 The average scaling exponent across cortical patches and participants
318 during Fixation (placebo only) was α = 0.67 (σ = 0.09) and during Task-counting
319 (placebo only) α = 0.64 (σ = 0.07), indicative of robust long-range temporal
320 correlations during both behavioral contexts. Averaged across all cortical voxels
321 and across Fixation and Task-counting conditions, there was a highly significant
322 increase in α (p = 0.0068; t = 2.93; paired t-test) under atomoxetine (α = 0.67, σ
323 = 0.05), compared to placebo (α = 0.65, σ = 0.05; Fig 5A). There was no
324 evidence for any effect of donepezil (α = 0.66, σ = 0.05) compared to placebo (p
325 = 0.50; t = 0.68; bf = 0.68; paired t-test; Fig 5A). The increase in scaling exponent
326 α under atomoxetine was widespread, but not homogenous across cortex,
327 comprising occipital and posterior parietal as well as a number of cortical regions
328 in the midline (Fig 5B, p = 0.0022; cluster-based permutation test).
329 The atomoxetine effect was, although subtle, highly reproducible across
330 runs. We tested this using a cross-validation approach. We first obtained a set of
331 voxels that were significantly increased under atomoxetine compared to placebo

(paired t-test, $p < 0.05$) during run 1 (averaged across the two behavioral contexts, Fixation and Task-counting). Next, we extracted the average scaling exponents across subjects for both conditions (atomoxetine and placebo) from run 2. We repeated the procedure with a set of voxels obtained from run 2 and extracted the scaling exponents from run 1. This unbiased approach reveals a highly significant increase in scaling exponent α after the administration of atomoxetine compared to placebo ($p = 0.0023$; $t = 3.365$; Fig 5D).

Repeating the spatial comparison separately for Fixation and Task-counting yielded significant effects of atomoxetine on α during both behavioral contexts (Fig 6A, Fixation: $p = 0.0245$; Fig 6B, Task-counting: $p = 0.0035$; cluster-based permutation test). The significant atomoxetine effects occurred in largely overlapping posterior cortical regions (Fig 6C). Conversely, we found no evidence for a significant interaction between the effects of atomoxetine and task anywhere in cortex: A direct comparison of the atomoxetine vs. placebo contrast maps between Fixation and Task-counting yielded no significant clusters ($p > 0.081$ for all clusters; cluster-based permutation test). Taken together, these results indicate that the effects of atomoxetine were largely independent of sensory drive and behavioral context.

By contrast, we found no significant effect of donepezil on α in any cortical region ($p > 0.22$ for all clusters; cluster-based permutation test; Fig 5C). Further, no effects were evident for donepezil, when splitting by task conditions (Fig S4). The control analyses presented below establish clear effects of donepezil on both cortical activity as well as markers of peripheral nervous system activity, thus ruling out concerns that the drug may have been less effective overall than atomoxetine (see Discussion).

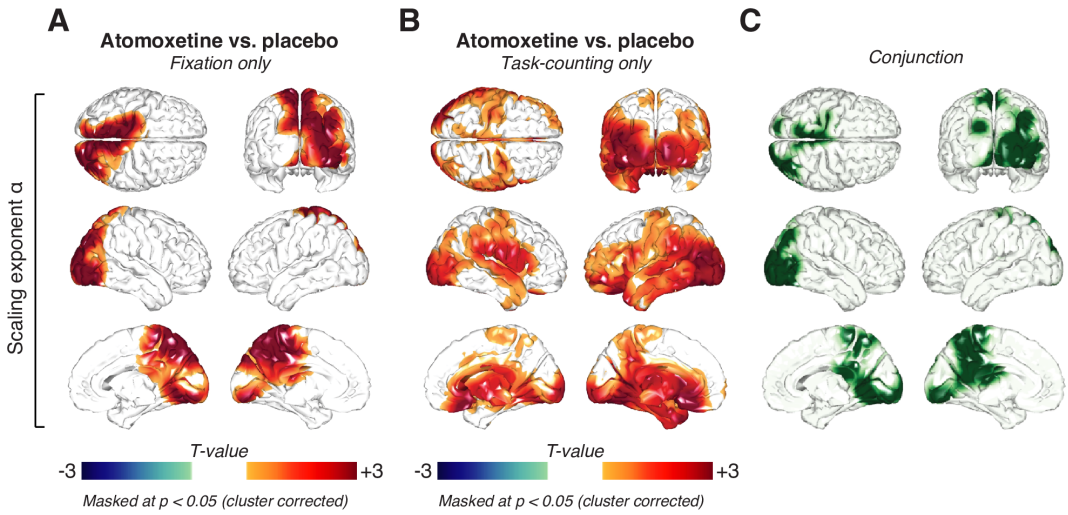

Fig 6. Atomoxetine increases long-range temporal correlations irrespective of behavioral condition**.** Spatial distribution of the atomoxetine-induced changes in scaling exponent α during **(A)** Fixation and **(B)** Task-counting. **(C)** Conjunction of maps in (A) and (B), highlighting (in green) voxels with significant increases in both conditions.

Decreased scaling exponent of cortical activity during Task-counting

The cortex-wide scaling exponent α was significantly larger during Fixation than during Task-counting (p = 0.0062; t = 2.97; paired t-test; placebo condition only). This difference was significant across large parts of cortex ($p < 0.05$; cluster-based permutation test; Fig 7A). The task-related decrease was also observed consistently across all pharmacological conditions (Fig 7A). Importantly, the regions exhibiting significant decreases during Task-counting included the occipital and parietal regions that were driven by the moving stimulus and exhibited atomoxetine-induced changes in scaling behavior. Indeed, when testing for the task-dependent change in scaling exponent specifically in those regions showing a significant atomoxetine effect, the reduction during Task-counting was also highly significant (Fig 7B).

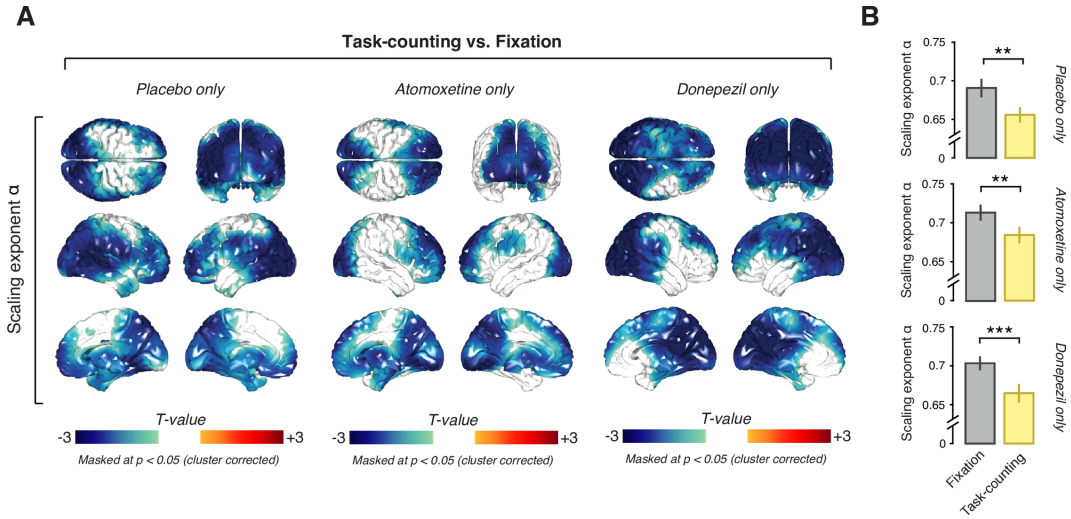

Fig 7. Decreased long-range temporal correlations under Task-counting **(A)** Difference in scaling exponent α between Task-counting and Fixation. *Left:* Contrast only for Placebo condition. *Middle.* Contrast only for Atomoxetine condition. *Right.* Contrast only for Donepezil condition. **(B)** Scaling exponent α for Fixation (purple) and Task-counting (yellow) conditions, averaged across voxels comprising the conjunction cluster depicted in Fig. 6C for placebo only (*Top*), atomoxetine only *(Middle)* and donepezil only *(Bottom).*

Change in scaling exponent under atomoxetine is consistent with increase in net cortical E/I ratio

In our model, the scaling exponent α exhibited a non-monotonic dependence on excitation-inhibition ratio (see the white diagonal line in Fig 4G-I and schematic depiction in Fig 8). Consequently, without knowing the baseline state, any change in α is ambiguous with respect to the direction of the change in E/I ratio (i.e., towards excitation- or inhibition-dominance). Thus, the observed increase in α under atomoxetine during Fixation could have been due to either an increase or a decrease in E/I ratio. However, recent insights into the changes in visual cortical E/I ratio during sensory drive in rodents help constrain the baseline state during the Task-counting condition: In the awake state, counter-intuitively, sensory drive decreases E/I ratio in primary visual cortex (33,34). Assuming that the same holds in human cortex during the Task-counting condition this insight enabled us to infer the change in net cortical E/I ratio induced by atomoxetine during Task-counting.

The rationale is illustrated in Fig 8. The observed decrease in α during Task-counting compared to Fixation (Fig 7A) was likely due to a shift towards inhibition-dominance (yellow point in Fig 8A). Then, the atomoxetine-induced increase in α during this condition was likely due to an increase in net E/I ratio during Task-counting (Fig 8B) – the same conclusion inferred from the increase in the rate of perceptual alternations above. Because the effects of atomoxetine on α were the same during Task-counting and Fixation, it is likely that the same mechanism was at play during Fixation, where the baseline state was unknown.

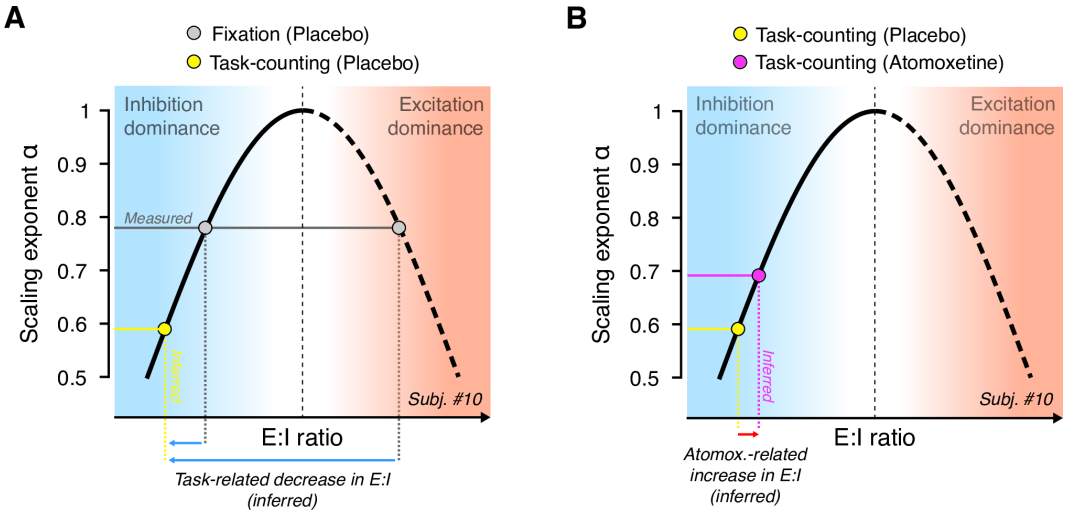

Fig 8. Inferring net E/I ratio from changes in scaling exponent α. Schematic illustration of the inference from observed change in exponent to (hidden) change in net E:I ratio (see main text for details). The non-monotonic dependence of scaling exponent α on E:I ratio (white line in Fig 4H) is replotted schematically. **(A)** The measured scaling exponent α during Fixation (gray) can result from both, inhibition- or excitation-dominant regimes; the baseline is unknown. We assume that external drive (Task-counting; yellow dot) does not increase E:I ratio (Shadlen & Newsome, 1998). Thus, the observed decrease in scaling exponent during Task-counting (yellow) must reflect a shift towards the inhibition-dominance (blue arrows), consistent with animal physiology (34). **(B)** This constrains the baseline state for the interpretation of the atomoxetine-induced increase in scaling exponent during Task-counting (red): The latter increase likely reflects an increase in E:I ratio (red arrow).

Distinct, or absent, drug effects on other features of cortical dynamics

The absence of a consistent change in the scaling behavior of cortical activity fluctuations under donepezil (Fig 5C) was not simply due to a lack of effect on cortical dynamics per se. During Fixation, atomoxetine and donepezil both significantly reduced MEG power in the 8-12 Hz range, relative to placebo, in

posterior cortical regions (Fig 9 A/B; $p < 0.05$ for all clusters; two-sided cluster-based permutation test). This suppression in cortical 8-12 Hz power due to both catecholamines and acetylcholine during Fixation is largely consistent with previous pharmacological work (30,40), as well as with correlations of cortical activity with pupil diameter (41–44), a marker of neuromodulatory brainstem activity underlying the release of noradrenaline and, to some extent, acetylcholine (45–48).

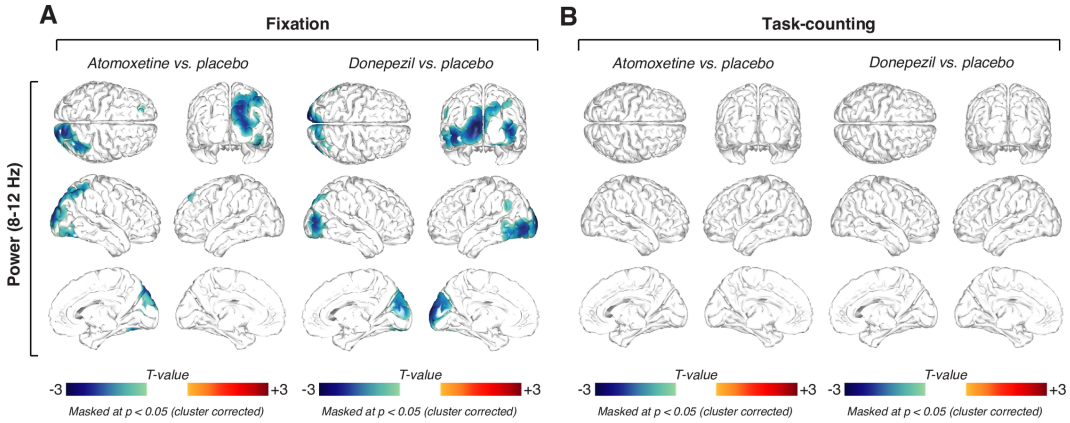

Fig 9. Similar effects of atomoxetine and donepezil on 8-12 Hz power. **(A)** Spatial distribution of drug-related alpha power changes during Fixation, thresholded at $p = 0.05$ (two-sided cluster-based permutation test). *Left.* Power changes after the administration of atomoxetine. *Right.* Power changes after the administration of donepezil. **(B)** Same as (A), but for Task-counting.

The atomoxetine-induced changes on 8-12 Hz power during Fixation had a different spatial pattern than those of the atomoxetine-induced changes in the scaling exponent α: within the cluster of the significant main effect of atomoxetine on α, power did not significantly correlate with the changes in α (group average spatial correlation between pooled difference maps within cluster; $r = 0.073$; $p = 0.129$, $bf = 1.065$).

During Task-counting, neither drug significantly altered MEG-power (Fig 9B, $p > 0.05$ for all clusters; two-sided cluster-based permutation test), presumably due to the already suppressed power in the 8-12 Hz range in that condition.

In sum, the effects of the drugs on cortical power during both conditions showed that both were, at the dosages selected for our study, were equally effective on cortical dynamics, consistently suppressing the power of low-frequency oscillations during Fixation. This, as well as the lack of spatial correlation of the atomoxetine-induced effects on power and scaling exponent α further supports the specificity of the atomoxetine effect on cortical scaling behavior.

Atomoxetine effect on fluctuations in cortical activity is not due peripheral confounds

We also controlled for changes in peripheral physiological signals under the drugs as potential confounds of the effect on cortical scaling behavior (Fig 10). As expected, atomoxetine increased average heart rate (Fig 10A,B). Donepezil had no significant effect on average heart rate, during neither Fixation ($p = 0.8676$; $t = 0.16$; paired t-test; $bf = 0.8676$; Fig 10A) nor Task-counting ($p = 0.3274$; $t = 1.0$; paired t-test; $bf = 0.3139$; Fig 10B). Both drugs, however, significantly altered heart rate scaling behavior, increasing the scaling exponent α (computed on inter-heartbeat-interval time series, see Methods) in both behavioral contexts (Fixation/atomoxetine: $p = 0.0012$, $t = 3.62$; Task-counting/atomoxetine: $p = 0.0167$; $t = 2.55$; Fig 10C; Fixation/donepezil: $p = 0.0076$, $t = 2.88$; Task-counting/donepezil: $p = 0.0049$, $t = 3.06$; Fig 10D; all paired t-tests). Critically, the atomoxetine-induced changes in heart rate showed no (Task-counting: $r = 0.00$; $p = 0.99$; Person correlation; $bf = 0.15$) or only weak and statistically non-significant (Fixation: $r = 0.24$; $p = 0.21$; Person correlation; $bf = 0.31$) correlations with the changes in cortical activity (Fig 10A/B, right). Similarly, the atomoxetine-related changes in the scaling behavior of inter-heartbeat intervals were only weakly (and

not significantly) correlated with the changes in cortical scaling behavior (Fixation: r = 0.22; p = 0.26; bf = 0.27; Task-counting: r = 0.26; p = 0.19; bf = 0.35; Fig 10C/D, right).

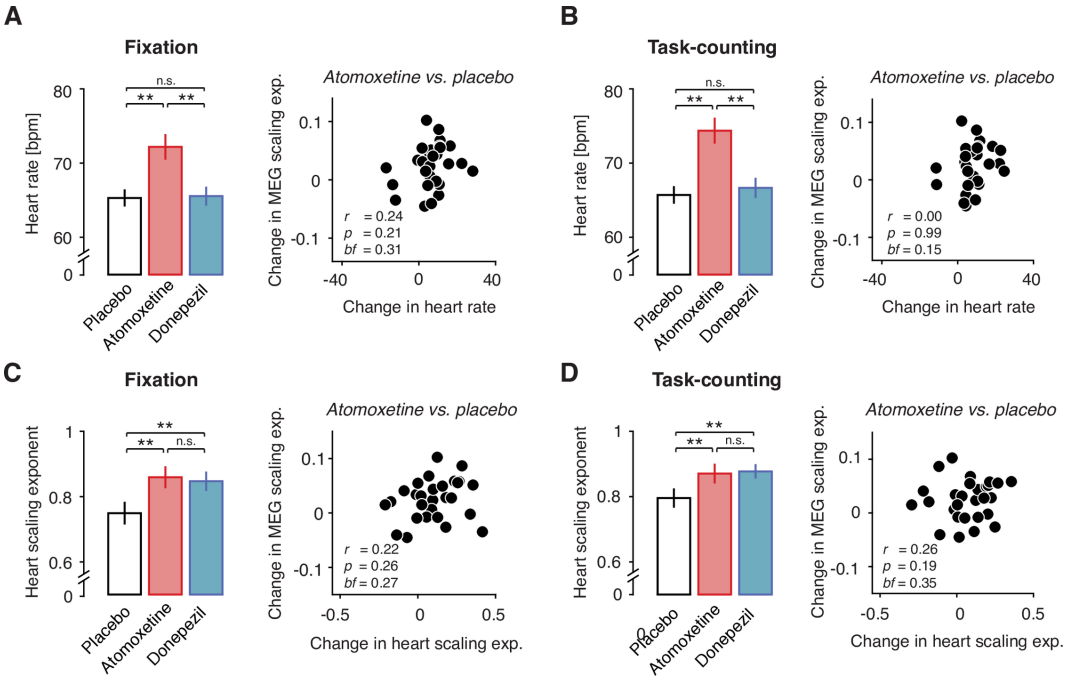

Fig 10. Drug effect on cortical scaling behavior is not explained by systemic drug effects**. (A)** *Left.* Heart rate for atomoxetine, placebo and donepezil during Fixation. *Right.* Correlation of atomoxetine-related changes in heart rate (x-axis) with atomoxetine-related changes in MEG scaling exponent α (y-axis) (within significant cluster during Fixation). **(B)** As (A), but during Task-counting **(C)** *Right.* Scaling behavior of inter-heartbeat intervals (heart scaling exponent). *Left.* Heart scaling exponent for all pharmacological conditions during Fixation. *Right.* Correlation of atomoxetine-related changes in heart scaling exponent (x-axis) with atomoxetine-related changes in MEG scaling exponent α (y-axis). **(D)** Same as (C), but during Task-counting.

Atomoxetine, but not donepezil, significantly decreased spontaneous blink rate during Fixation (p = 0.034; t = 2.24; paired t-test), but not during Task-counting (p = 0.112; t = 1.645; bf = 1.130; paired t-test; Fig S2B). However, again there was no significant correlation between changes in blink-rate and changes in cortical scaling behavior due to atomoxetine (Fixation: r = -0.26; p = 0.19; bf = 0.35; Task-counting: r = -0.09; p = 0.64; bf = 0.16).

In sum, drug-induced changes in peripheral physiological signals under the drugs, if present, did not account for the atomoxetine-induced changes in the scaling behavior of the fluctuations in cortical activity (Figs 5 and 6). These controls support our interpretation in terms of a specific effect on cortical net E/I

ratio rather than non-specific secondary effects due to the systemic drug effects or changes in retinal input due to blinks.

DISCUSSION

Cortical circuits maintain a tight balance between excitation and inhibition. The E/I ratio shapes the computational properties of cortical neurons and circuits (49), and thereby the behavior of the organism (18–20). Deviations from this balance have been linked to schizophrenia and autism and might also be at play in various other neuropsychiatric disorders (50–53). Even in the absence of changes in sensory input, the ratio between excitation and inhibition changes continuously in cortex (17,54), presumably due to the effects of neuromodulators, such as noradrenaline and acetylcholine (20,27–29,55,56). Neuromodulators also regulate ongoing changes in the operating mode of behavior (23,25,57,58). Here, we unraveled the effect of neuromodulatory-controlled microcircuit level changes on the net cortical E/I ratio, as manifest in perception and behavior as well as in local cortical population dynamics. Catecholamines, but not acetylcholine, altered both, the dynamics of perceptual inference in the face of ambiguous input, and intrinsic fluctuations in cortical activity. Both effects provided independent and convergent evidence for an increase in E/I ratio due to catecholamines.

Convergent evidence for catecholaminergic disinhibition in cortical circuits

Our simulations indicated that the long-range temporal correlation of neural population activity, as measured with the scaling exponent α, was highly sensitive to changes in E/I ratio, produced through different regimes of asymmetric synaptic gain modulation (see the white line in Fig 4H). In both versions of our model, the neuromodulatory effects were not perfectly symmetric

(see the deviations of peak scaling exponents from main diagonal in Fig 4H). While the latter effect was small and may be specific to the particular details of the model, it remains possible that the subtle changes in scaling exponents we observed were produced through symmetric gain modulations that maintained the net E/I balance (i.e., along the main diagonal). However, two additional lines of evidence converge on our conclusion that catecholamines (in particular noradrenaline) boosted the cortical E/I ratio.

The first line of evidence is the specific and consistent effect of the cathecolaminergic manipulation on perceptual switch rate in same group of participants. Building on a well-documented link between the volatility of perceptual inference on cortical net E/I-balance (21,31,32), this behavioral effect sits well with the notion of an effective net disinhibition in the circuits of visual cortex that determine the dynamics of perceptual inference in the face of ambiguous motion signals.

Second, a mounting body of evidence from recent invasive rodent work also supports an overall increase in net cortical E/I ratio due to catecholamines, specifically noradrenaline (17). One study established that noradrenaline decreases tonic, ongoing inhibition of neurons in auditory cortex, with the excitatory inputs unaffected (56). Another study showed that noradrenaline (but not acetylcholine) mediated a locomotion-related, tonic depolarization of visual cortical neurons (including pyramidal cells) (27). Both studies indicated a non-selective (i.e. broadband) gain increase of neuronal responses, irrespective of the features of presented stimuli, which is different from the more subtle disinhibitory effects of acetylcholine (17,55).

Cortical distribution of catecholaminergic effects on activity fluctuations

552 The atomoxetine effects on the scaling exponent were widespread across cortex,
553 but not entirely homogenous. They were pronounced across occipital and parietal
554 cortex, but not robust in frontal cortex (see Fig 5B). This distribution might point to
555 a noradrenergic, rather than dopaminergic origin. Atomoxetine increases the
556 levels of both catecholamines, noradrenaline and dopamine (59), but the
557 dopaminergic system mainly projects to prefrontal cortex (60) but only sparsely
558 projects to occipital areas (61), whereas the noradrenergic projections are more
559 widespread and strong to occipito-parietal cortex (62). Alternatively, this
560 distribution may reflect the different receptor composition of across cortical
561 regions (63,64): The relative frequency of different adrenoceptors (α1-, α2 or β-
562 adrenoceptor) differs strongly between frontal and posterior cortex, which, in turn,
563 can result in distinct effects of noradrenaline on the dynamics of neural activity in
564 these different cortical regions (63), in particular persistent activity. Future studies
565 should investigate whether the observed differences of noradrenergic effects on
566 long-range temporal correlations in cortical activity are due to these differences in
567 adrenoceptor composition across cortex.

568

569 **No evidence for cholinergic effects on net E/I ratio**

570 In contrast to atomoxetine, we observed no robust effect of increased
571 acetylcholine levels on cortical long-range temporal correlations. This absence of
572 an effect was unlikely due to an ineffective pharmacological manipulation through
573 donepezil: the latter had equally strong effects as atomoxetine on alpha-band
574 power in some cortical regions, as well as on heart rate variability. Rather, the
575 absence of robust donepezil effects might reflect specific properties of cholinergic
576 action, which may leave the cortical net excitation-inhibition ratio largely
577 unchanged. Substantial evidence points to the rapid disinhibition of (excitatory)

pyramidal cells by acetylcholine, by activating a circuit made up of a chain of two inhibitory interneurons (VIP+ and SOM+) (28,65,66). The cholinergic activation of this disinhibitory circuit would be expected to shift the net excitation-inhibition ratio towards excitation, just as we inferred for catecholamines. However, this disinhibitory circuit seems to mainly affect transient, stimulus-evoked responses (55), whereas noradrenaline also alters the tonic levels of inhibition (56). This may explain the relative lack of donepezil effects during the steady-state conditions (blank fixation and continuous task drive) employed in our present study. In general, cholinergically mediated disinhibitory effects on cortical neurons might be subtler as well as more selective than the ones mediated by noradrenaline (17).

Decrease of long-range temporal correlations during task and sensory drive

Consistent with our current results, previous studies also found a decrease in temporal autocorrelations of cortical activity due to external drive, even during intermittent presentation of stimuli and tasks, entailing more external transients than the steady-state task condition used here (8,67). The observation is consistent with the insight from intracellular recordings of cortical neurons in animals, that cortical responses to sensory stimulation in the awake state are dominated by inhibition (33,34). One candidate source of this sensory-driven state change is thalamocortical inhibition (68), but intracortical feedback inhibition might also contribute (69).

Simulations of large-scale biophysical models of cortical networks show that the driven state is associated with shortened temporal autocorrelations as well as a decrease in the entropy of activity states in the network (70).

Correspondingly, the increase in long-range temporal autocorrelations under catecholaminergic modulation observed presently may be associated with an increase in entropy, in other words, a tendency of the cortex to explore a larger set of activity states. This greater exploration of cortical state space may in turn be linked to a prominent idea about the function of noradrenaline, which postulates that high tonic noradrenaline levels promote exploratory, and more distractible, behavior (23).

Functional consequences of changes in net cortical E/I ratio

We observed a selective increase in the rate of spontaneous perceptual alternations under catecholaminergic but not cholinergic boost, adding to evidence that these dynamics are under neuromodulatory control (71). Such a change could be due to an increase in cortical “noise” defined as the amplitude of spontaneous fluctuations in activity (31). Future invasive studies should relate chatecholaminergic changes in the variability of spiking activity (72) to bistable perception.

The selective increase of perceptual alternation rate under atomoxetine is consistent with the relative decrease of intra-cortical inhibition (21) that was also inferred from the changes in the long-range temporal correlation structure of cortical activity. A net increase in excitation will likely have particularly strong effects on the dynamics of parietal and prefrontal cortical circuits involved in working memory and decision-making (19). These circuits are characterized by slow intrinsic fluctuations of activity (73–75). The catecholaminergic increase in long-range temporal correlations of intrinsic activity fluctuations in parietal circuits that we observed in the current study may reflect a relative increase specifically in the recurrent excitation in ‘accumulator’ circuits. Recurrent excitation, in turn, is

essential for both the computational capacities (76) as well as the timescale of intrinsic activity fluctuations of these circuits (74,75). Simulations of synaptic gain modulation of such 'accumulator' circuits indicate that the most robust behavior emerges from co-modulation of both excitatory and inhibitory synapses, but with different factors (20). It will be important to test these predictions in future work, using tasks tailored to probing into these circuits of association cortex.

Catecholamines: a control parameter for critical network dynamics

Long-range temporal correlations in the fluctuations of neural mass activity (i.e., activity summed across the entire local network) (7) and avalanches within the neuronal network (37) jointly emerge at the same ratio between excitatory and inhibitory connectivity in the simplified cortical patch model used here. Both phenomena, long-range temporal correlations and neuronal avalanches, are commonly interpreted as hallmarks of "criticality" (7,10,37,77). Criticality refers to a complex dynamical system poised between order and chaos (78–80).

The cortex might operate in a narrow regime around this critical point (80,81). This operating mode, in turn, might yield computational modes superior to those of the "sub-" or "supercritical" modes (38,77,82–84). A number of recent reports have indicated that cortical dynamics may fluctuate around the critical state (85–88), but these fluctuations have, so far, been spontaneous. Here, we identified two key factors (task drive and catecholaminergic neuromodulation) to bring these changes under experimental control. Complex systems can self-organize towards criticality (78), e.g., through plasticity and/or feedback connections. However, critical dynamics can also be achieved through an external control parameter that fine-tunes the system. The tuning of temperature

in the Ising model of spin magnetization is a common example (80). Noradrenaline may serve as such a control parameter in the cerebral cortex.

In sum, combining measurements of perceptual dynamics as well as intrinsic fluctuations in cortical population activity under steady-state perceptually ambiguous stimulation provides a novel non-invasive read-out of pharmacological effects on cortical net E/I ratio in humans. This read-out might be useful for addressing fundamental questions about the state dependence of cortical computation and for inferring changes in cortical E/I ratio in neuropsychiatric disorders, or pharmacological treatments of these disorders.

METHODS

Pharmacological MEG experiment

Participants

30 healthy human participants (16 females, age range 20-36, mean 26.7) participated in the study after informed consent. The study was approved by the Ethical Committee responsible for the University Medical Center Hamburg-Eppendorf. Two participants were excluded from analyses, one due to excessive MEG artifacts, the other due to not completing all 3 recording sessions. Thus, we report results from N=28 participants (15 females).

General design

We pharmacologically manipulated the levels of catecholamines (noradrenaline and dopamine) and acetylcholine in a double-blind, randomized, placebo-controlled, and cross-over experimental design (Fig 1A, B). Each participant completed three experimental sessions, consisting of drug (or placebo) intake at two time points, a waiting period of 3 hours, and an MEG recording. During each

MEG session, participants were seated on a chair inside a magnetically shielded MEG chamber. Each session consisted of 6 runs of different tasks, each of which was 10 minutes long and followed by breaks of variable duration.

Pharmacological intervention

We used the selective noradrenaline reuptake inhibitor atomoxetine (dose: 40 mg) to boost the levels of catecholamines, specifically noradrenaline and (in prefrontal cortex) dopamine (59). We used the cholinesterase inhibitor donepezil (dose: 5 mg) to boost acetylcholine levels. A mannitol-aerosil mixture was administered as placebo. All substances were encapsulated identically in order to render them visually indistinguishable. Peak plasma concentration are reached ~3-4 hours after administration for donepezil (89) and 1-2 hours after administration for atomoxetine (90), respectively. We adopted the following procedure to account for these different pharmacokinetics (Fig 1A): participants received two pills in each session, one 3 h and another 1.5 h before the start of MEG recording. In the Atomoxetine condition, they first received a placebo pill (t = -3 h) followed by the atomoxetine pill (t = -1.5 h). In the Donepezil condition, they first received the donepezil pill (t = -3 h), followed by placebo (t = -1.5 h). In the Placebo condition, they received a placebo at both time points. The half-life is ~ 5 h for atomoxetine (90) and ~ 82 h for donepezil, respectively (89). In order to allow plasma concentration levels to return to baseline, the three recording sessions were scheduled at least 2 weeks apart. This design ensured maximum efficacy of both pharmacological manipulations, while effectively blinding participants as well as experimenters.

Stimuli and behavioral tasks

In each session, participants alternated between three different task conditions (2 runs à 10 minutes per condition) referred to as Fixation, Task-counting, and Task-pressing in the following (Fig 1B). All conditions entailed overall constant sensory input. Fixation and Task-counting also entailed no overt motor responses and are, therefore, referred to as "steady-state" conditions in the following. We used these steady-state conditions to quantify intrinsic fluctuations in cortical activity. Task-pressing entailed motor responses and was used for reliable quantification of perceptual dynamics. All instructions and stimuli were projected onto a screen (distance: 60 cm) inside the MEG chamber. The individual conditions are described as follows.

Fixation. Participants were asked to keep their eyes open and fixate a green fixation dot (radius = 0.45° visual angle) presented in the center of an otherwise gray screen. This is analogous to eyes-open measurements of "resting-state" activity widely used in the literature on intrinsic cortical activity fluctuations.

Task-counting. Participants viewed a seemingly rotating sphere giving rise to the kinetic depth effect (91,92): spontaneous changes in the perceived rotation direction (Fig 1B). The stimulus subtended 21° of visual angle. It consisted of 1000 dots (500 black and 500 white dots, radius: 0.18° of visual angle) arranged on a circular aperture presented on a mean-luminance gray background, with the green fixation dot in the center. In order to minimize tracking eye movements, the sphere rotation was along the horizontal axis, either "forward" (towards the observer) or "backward" (away from the observer), and the dot density decreased along the horizontal axis towards the center of the stimulus. Participants were instructed to count the number of perceived changes in rotation direction and report the total number of perceived transitions at the end of the run. Just like

during Fixation, Task-counting minimized any external (sensory or motor) transients. Subjects silently counted the alternations in perceived rotation direction and verbally reported the total count after the end of the 10 min run.

Task-pressing. This condition was identical to Task-counting, except that participants were instructed to press and hold one of two buttons with their index finger to indicate the perceived rotation direction of the sphere. Thus, each perceptual alternation was accompanied by a motor response leading to change in the button state. This allowed for a more reliable quantification of participants' perceptual dynamics. On two sessions (atomoxetine condition), button presses were not registered. Hence, the corresponding analyses were performed on 26 participants.

Data acquisition

MEG was recorded using a whole-head CTF 275 MEG system (CTF Systems, Inc., Canada) at a sampling rate of 1200 Hz. In addition, eye movements and pupil diameter were recorded with an MEG-compatible EyeLink 1000 Long Range Mount system (SR Research, Osgoode, ON, Canada) at a sampling rate of 1000 Hz. In addition, electrocardiogram (ECG) as well as vertical, horizontal and radial EOG were acquired using Ag/AgCl electrodes (sampling rate 1200 Hz).

Data analysis

Eye data

Eye blinks were detected using the manufacturer's standard algorithm with default settings. Saccades and microsaccades were detected using the saccade detection algorithm described in (93), with a minimum saccade duration of 4

758 samples (= 4 ms) and a threshold velocity of 6. For 18 out of 28 participants, only
759 horizontal eye movements were recorded.
760
761 *EOG data*
762 EOG events (blinks and saccades) were extracted using semi-automatic artifact
763 procedures as implemented in FieldTrip (94). In short, EOG traces were
764 bandpass filtered using a third-order butterworth filter (1 – 15 Hz) and the
765 resulting signal was z-scored. All time points where the resulting signal exceeded
766 a z-score of 4 were marked as an EOG event.
767
768 *MEG data*
769 *Preprocessing.* First, all data were cleaned of strong transient muscle artifacts
770 and squid jumps through visual inspection and manual as well as semi-automatic
771 artifact rejection procedures, as implemented in the FieldTrip toolbox for MATLAB
772 (94). To this end, data segments contaminated by such artifacts (+/- 500 ms)
773 were discarded from the data (across all channels). Subsequently, data were
774 downsampled to 400 Hz split into low (2-40 Hz) and high (>40 Hz) frequency
775 components, using a 4th order (low- or high-pass) Butterworth filter. Both signal
776 components were separately submitted to independent component analysis (95)
777 using the FastICA algorithm (96). Artifactual components (eye blinks/movements,
778 muscle artifacts, heartbeat and other extra-cranial artifacts) were identified based
779 on three established criteria (97): power spectrum, fluctuation in signal variance
780 over time (in bins of 1s length), and topography. Artifact components were
781 reconstructed and subtracted from the raw signal and low- and high frequencies
782 were combined into a single data set. On average, 20 (+/- 14) artifact

783 components were identified for the low frequencies and 13 (+/- 7) artifactual
784 components were identified for the high frequencies.
785
786 *Spectral analysis*. Sensor-level spectral estimates (power spectra and cross
787 spectral density matrices) were computed by means of the multi taper method
788 using a sequence of discrete prolate Slepian tapers (98). For the power spectrum
789 shown in Fig 1C, power spectra were computed using a window length of 5s and
790 a frequency smoothing of 2 Hz, yielding 19 orthogonal tapers. The focus of this
791 paper was on the fluctuations of the amplitude envelopes, rather than on the
792 (oscillatory) fluctuations of the carrier signals *per se*. The temporal correlation
793 structure of the amplitude envelope fluctuations of cortical activity seems similar
794 across different carrier frequency bands (10). We focused on amplitude envelope
795 fluctuations in the alpha-band because (i) the cortical power spectra exhibited a
796 clearly discernible alpha-peak, which robustly modulated with task, as expected
797 from previous work (39) (Fig 1C); and (ii) the computational model used to study
798 the effect of synaptic gain modulation on cortical activity fluctuations was tuned to
799 produce alpha-band oscillations (see above and (15)).
800
801 *Source reconstruction: general approach*. The cleaned sensor level signals (N
802 sensors) were projected onto a grid consisting of $M = 3000$ voxels covering the
803 cortical surface (mean distance: 6.3 mm) using the exact low-resolution brain
804 electromagnetic tomography (eLORETA; (99) method. The magnetic leadfield
805 was computed, separately for each subject and session, using a single shell head
806 model constructed from the individual structural MRI scans and the head position
807 relative to the MEG sensors at the beginning of the run (100). In case no MRI
808 was available (4 subjects), the leadfield was computed from a standard MNI

809 template brain transformed to an estimate of the individual volume conductor
810 using the measured fiducials (located at the nasion, the left and the right ear).
811
812 *Source level estimates of amplitude envelopes and power*. For comparing
813 amplitude envelope and power estimates between experimental conditions in
814 source space we aimed to select a single direction of the spatial filter for each
815 voxel across pharmacological conditions (i.e., MEG sessions), but separately for
816 Fixation and Task-Counting conditions. The rationale was to avoid filter-induced
817 biases in the comparisons between the pharmacological conditions, while
818 allowing that external task drive might systematically change the dipole
819 orientations.
820 To this end, we first computed the mean source-level cross-spectral
821 density matrix $C(r,f)$ for each frequency band, f, averaged across the three
822 MEG sessions, as follows:
823 $$C(r,f) = \frac{1}{3}\sum_{i=1}^{3}\left(A_i^T(r)C_i(f)A_i(r)\right) \quad (1)$$
824 whereby i indicated the MEG session, $C_i(f)$ was the (sensor-level) session- and
825 frequency-specific cross-spectral density matrix and A_i is the spatial filter for
826 session i. We then extracted the first eigenvector $u_1(r,f)$ of the session-average
827 matrix $C(r,f)$ and computed the unbiased filter selective for the dominant dipole
828 orientation, $B_i(r,f)$, as:
829 $$B_i(r,f) = A_i(r)u_1(r,f) \quad (2)$$
830 Please note that this filter was now frequency-specific, whereas the
831 previous filters, $A_i(r)$, were not. To obtain instantaneous estimates of source-
832 level amplitudes, the sensor-level signal for session i, $X_i(t)$, was band-pass
833 filtered (using a finite impulse response filter) and Hilbert-transformed, yielding a
834 complex-valued signal $H_i(f,t)$ for each frequency band. This signal was

projected into source space through multiplication with the unbiased spatial filter, $B_i(r,f)$, and the absolute value was taken:

$$Env_i(r,f,t) = |\big(H_i(f,t)\ B_i(r,f)\big)| \qquad (3)$$

where $Env_i(r,f,t)$ was the estimated amplitude envelope time course of source location r and frequency f. Next, for each session, unbiased source-level cross spectral density estimates were obtained from the sensor-level cross-spectral density matrix $C_i(f)$ and the frequency-specific, unbiased spatial filter $B_i(f)$. The main diagonal of the resulting matrix contains source-level power estimates for all source locations:

$$S_i(f) = diag(B_i^T(f)_i C_i(f) B_i(f)) \qquad (4)$$

These computations where repeated separately for the Task-counting and Fixation conditions, session by session. The differences in amplitude envelope fluctuations and power estimates between pharmacological and task conditions reported in this paper were robust with respect to the specifics of the analysis approach. In particular, we obtained qualitatively similar pharmacological effects in sensor space, as reported in an earlier conference abstract (101).

Detrended fluctuation analysis. The source-level amplitude envelopes $Env_i(r,f,t)$ were submitted to detrended fluctuation analysis (102,103) in order to quantify long-range temporal correlations. Detrended fluctuation analysis quantifies the power law scaling of the fluctuation (root-mean-square) of a locally detrended, cumulative signal with time-window length. Different from the analysis of the more widely known autocorrelation function (73,74), detrended fluctuation analysis provides robust estimates of the autocorrelation structure for stationary and non-stationary time series. The procedure of the detrended fluctuation analysis is illustrated in Fig 2.

For simplicity, in the following, we re-write the amplitude envelope $Env_i(r,f,t)$ as x of length T. First, we computed the cumulative sum of the demeaned x, (Fig 2B):

$$X(t) = \sum_{t'=1}^{t}(x(t') - \langle x \rangle) \quad (5)$$

where t' and t denote single time points up to length T. The cumulative signal X was then cut into $i = 1 \ldots k$ segments Y_i of length N (overlap: 50%), where $k = floor[(T-N)/(0.5\,N)]$ (Fig 2B, top). Within each segment Y_i of equal length N, the linear trend Y_{i_trend} (least squares fit) was subtracted from Y_i (Fig 2B, bottom, blue vs. red lines), and the root-mean-square fluctuation for a given segment was computed as:

$$F_{N\_i} = \left[\frac{1}{N}\sum_{n=1}^{N}(Y_i(n) - Y_{i\_trend}(n))^2\right]^{\frac{1}{2}} \quad (6)$$

where n indicates the individual time points. The fluctuation was computed for all k segments of equal length N and the average fluctuation was obtained through:

$$< F_N > = \frac{1}{k}\sum_{i=1}^{k} F_{N\_i} \quad (7)$$

The procedure was repeated for 15 different logarithmically spaced window lengths N, ranging from 3 s to 50 s, which yields a fluctuation function (Fig 2C). As expected for scale-free time series (103), this fluctuation function follows a power-law of the form:

$$< F_N > \propto N^{\alpha} \quad (8)$$

The "scaling exponent" α was computed through a linear regression fit in log-log coordinates (Fig 2C). The longest and shortest window lengths were chosen according to guidelines provided in (103).

A scaling exponent of $\alpha \sim= 0.5$ indicates a temporally uncorrelated ("white noise") process. Scaling exponents between $0.5 < \alpha < 1$ are indicative of scale-free behavior and long-range temporal correlations (103), whereas exponents of $\alpha < 0.5$ indicate long-range anti-correlations ("switching behavior") and $\alpha > 1$ are

887 indicative of an unbounded process (103). The scaling exponents for alpha-band
888 MEG amplitude envelopes estimated in this study ranged (across experimental
889 conditions, MEG sensors and participants) from 0.40 and 1.04, with 99.4% of all
890 estimates in the range from 0.5 to 1. This is indicative of scale-free behavior and
891 consistent with previous human MEG work (7–10,12,13).
892
893 *Relationship between measures of cortical variability*. Scale-free behavior of
894 neural time series has also been quantified via analysis of the power spectrum
895 (5,6,73). There is a straightforward relationship between both approaches, which
896 we explain below, to help appreciate our results in the context of these previous
897 studies. The power spectrum of the amplitude envelope of cortical activity is
898 typically well approximated by the power law $p(f) \propto f^{-\beta}$, where β is referred to
899 as the power-law exponent (Fig 2D). For power-law decaying autocorrelations,
900 the relationship between the power-law exponent β and the scaling exponent α
901 (estimated through DFA) of a time series is:
902 $$\beta = 2\alpha - 1 \qquad (9)$$
903
904 *Analysis of ECG data*. ECG data were used to analyze two measures of
905 peripheral autonomic activity: average heart rate and heart rate variability. For
906 both measures, we used an adaptive threshold to detect the R-peak of each
907 QRS-complex in the ECG. Heart rate was then computed by dividing the total
908 number of R-components by time. Heart rate variability was quantified by means
909 of the detrended fluctuations analysis described for MEG above, but now applied
910 to the time series of the intervals between successive R-peaks (9,10). In line with
911 the MEG analyses, we used windows ranging from 3 to 50 heartbeats (roughly
912 corresponding to 3–50 s).

913

914 *Statistical tests*

915 Statistical comparisons of all dependent variables between conditions were,
916 unless stated otherwise, performed using paired t-tests.

917 Null effects are difficult to interpret using regular null hypothesis
918 significance testing. The Bayes Factor addresses this problem by quantifying the
919 strength of the support for the null hypothesis over the alternative hypothesis
920 provided by the data, taking effect size into account. Wherever null effects were
921 conceptually important, results obtained from a regular (paired) t-test (104) and
922 Pearson correlations (105) were converted into corresponding Bayes Factors.

923 To map significant changes of scaling exponents α on the cortical surface,
924 we computed a non-parametric permutation test based on spatial clustering
925 (106,107). This procedure has been shown to reliably control for Type I errors
926 arising from multiple comparisons. First, a paired t-test was performed to identify
927 voxels with significant changes (voxel with $p < 0.05$). Subsequently, significant
928 voxels are combined into clusters based on their spatial adjacency. Here, a voxel
929 was only included into a cluster when it had at least two significant neighbors.
930 Subsequently, the t-values of all voxels comprising a cluster were summed,
931 which yields a cluster statistic (i.e., a cluster t-value) for each identified cluster.
932 Next, a randomization null distribution was computed using a permutation
933 procedure (N = 10.000 permutations). On each permutation, the experimental
934 labels (i.e., the pharmacological conditions) were randomly re-assigned within
935 participants and the aforementioned procedure was repeated. For each iteration,
936 the maximum cluster statistic was determined and a distribution of maximum
937 cluster statistics was generated. Eventually, the cluster statistic of all empirical
938 clusters was compared to the values obtained from the permutation procedure.

All voxels comprising a cluster with a cluster statistic smaller than 2.5% or larger than 97.5% of the permutation distribution were labeled significant, corresponding to a corrected threshold of α = 0.05 (two-sided).

Model simulations

To simulate the effects of synaptic gain modulation on cortical activity fluctuations, we extended a previously described computational model of a local cortical patch (15) by means of multiplicative modulation of synaptic gain. All features of the model were identical to those of the model by (15), unless stated otherwise. The model consisted of 2500 integrate-and-fire neurons (75% excitatory, 25% inhibitory) with local connectivity within a square (width = 7 units) and a connection probability that decayed exponentially with distance (Fig 4A). The dynamics of the units were governed by:

$$I_i = I_i + \sum_j N_{ij} W_{ij} S_j \qquad (10)$$

$$\tau_i \frac{dI_i}{dt} = I_0 - I_i \qquad (11)$$

where subscripts i, j indicated different units, N_{ij} was a multiplicative gain factor, W_{ij} were the connection weights between two units, and S_j a binary spiking vector representing whether unit *j* did or did not spike on the previous time step, and $I_0 = 0$. The connection weights were $W_{EE} = 0.0085$, $W_{IE} = 0.0085$, $W_{EI} = -0.569$ and $W_{II} = -2$ whereby subscript E indicated excitatory, subscript I indicated inhibitory, and the first and second subscript referred to the receiving and sending unit, respectively.

On each time step (*dt* = 1 ms), I_i was updated for each unit i, with the summed input from all other (connected) units *j* and scaled by a time constant $\tau_i = 9$ ms, which was the same for excitatory and inhibitory units. The probability of a unit generating a spike output was given by:

$$P_{si} = P_{si} + I_i \quad (12)$$

$$\tau_P \frac{dP_{si}}{dt} = P_0 - P_{si} \quad (13)$$

with the time constant for excitatory units $\tau_P = 6\,ms$ and for inhibitory $\tau_P = 12\,ms$. P_0 was the background spiking probability, with $P_0(exc.) = 0.000001\,[1/ms]$ and $P_0(inh.) = 0\,[1/ms]$. For each time step, it was determined whether a unit did or did not spike. If it did, the probability of that unit spiking was reset to $P_r(excitatory) = -2\,[1/ms]$ and $P_r(inhibitory) = -20\,[1/ms]$.

We used this model to analyze the dependency of two quantities on E/I ratio: (i) the power-law scaling of the distributions of the sizes of neuronal avalanches (37) estimated in terms of the kappa-index κ which quantifies the difference between an empirically observed event size distribution and a theoretical reference power-law distribution with a power-law exponent -1.5 (38), and (ii) the scaling behavior (scaling exponent α) of the amplitude envelope fluctuations of the model's local field potential. To this end, we summed the activity across all (excitatory and inhibitory) neurons to obtain a proxy of the local field potential. We band-pass filtered the local field potential in the alpha-band (8–12 Hz) and computed long-range temporal correlations in the alpha-band amplitude envelopes following the procedure described above (see *Detrended fluctuation analysis of MEG data*), using windows sizes ranging from 5 s to 30 s. For all simulations reported in this paper, we optimized the connection weights using Bonesa, a parameter tuning algorithm (108), such that the network exhibited alpha-band oscillations, long-range temporal correlations, and neuronal avalanches (see Discussion).

In order to assess the influence of structural excitatory and inhibitory connectivity on network dynamics (Figs 4D-F), we varied the percentage of units (excitatory and inhibitory) a given excitatory or inhibitory unit connects to within a

local area (7 units x 7 units; Fig 4A). These percentages were varied independently for excitatory and inhibitory units with a step size of 2.5%.

The gain factor N_{ij} was the main difference to the model described by (15). It was introduced to simulate the effects of neuromodulation on synaptic interactions in the cortical network (20). With all the above parameters fixed (42.5% excitatory connectivity, 75% inhibitory connectivity; small square in Figs 4D-F), we systematically varied the synaptic gain factors, in two different ways. In the first version, we only varied N_{EE} and N_{IE} to dynamically modulate the circuit's net E/I ratio (Fig 4B), in a way consistent with recent modeling of the effects of E/I ratio on a cortical circuit for perceptual decision-making (18). In the second version, we varied N_{EE}, N_{IE}, and N_{EI} (Fig S3A). Here, N_{EI} was modulated independently from N_{EE},and N_{IE}, which in turn were co-modulated by the same factor.

Per parameter combination, we ran 10 simulations, using the Brian2 spiking neural networks simulator (109). Each simulation was run for 1000 seconds, with a random initialization of the network structure and the probabilistic spiking. In this paper, we focus on the effects of neuromodulation on the scaling exponent α, which served as a reference for interpretation of the MEG effects.

ACKNOWLEDGEMENTS

The authors thank Christiane Reissmann for help with the data collection, as well as Sander Nieuwenhuis and Peter Murphy for helpful comments on the manuscript. This work was supported by the German Research Foundation (DFG): Heisenberg Professorship DO 1240/3-1 (to T.H.D.), and the Collaborative Research Center SFB 936 (Projects A2/A3, A7, Z3, to A.K.E., T.H.D., G.N., respectively), BMBF (Project 161A130, to A.K.E.); the Netherlands Organization

for Scientific Research (NWO, dossiernummer 406-15-256 to K.L.-H. and A.-E.A.)

AUTHOR CONTRIBUTIONS

Conceptualization: T.P., A.K.E., and T.H.D.; Experimental design: T.P. and T.H.D.; Model design: T.P., A-E.A., K.L-H., and T.H.D.; Investigation: T.P.; Formal analysis: T.P.; Model simulations: A.-E.A.; Writing - Original draft: T.P. and T.H.D.; Writing – Review & Editing: T.P., A-E.A., G.N., A.K.E., K.L-H., and T.H.D. - Funding Acquisition: K.L-H., A.K.E., and T.H.D.; Supervision: G.N., K.L-H., and T.H.D.

COMPTETING FINANCIAL INTERESTS

The authors declare no competing financial interests.

REFERENCES

1. Faisal AA, Selen LPJ, Wolpert DM. Noise in the nervous system. Nat Rev Neurosci. 2008 Apr;9(4):292–303.

2. Shadlen MN, Newsome WT. The variable discharge of cortical neurons: implications for connectivity, computation, and information coding. J Neurosci Off J Soc Neurosci. 1998 May 15;18(10):3870–96.

3. Fox MD, Snyder AZ, Vincent JL, Corbetta M, Van Essen DC, Raichle ME. The human brain is intrinsically organized into dynamic, anticorrelated functional networks. Proc Natl Acad Sci U S A. 2005 Jul 5;102(27):9673–8.

4. Deco G, Jirsa VK, McIntosh AR. Emerging concepts for the dynamical organization of resting-state activity in the brain. Nat Rev Neurosci. 2011 Jan;12(1):43–56.

5. Miller KJ, Sorensen LB, Ojemann JG, den Nijs M. Power-law scaling in the brain surface electric potential. PLoS Comput Biol. 2009 Dec;5(12):e1000609.

6. He BJ, Zempel JM, Snyder AZ, Raichle ME. The temporal structures and functional significance of scale-free brain activity. Neuron. 2010 May 13;66(3):353–69.

7. Linkenkaer-Hansen K, Nikouline VV, Palva JM, Ilmoniemi RJ. Long-range temporal correlations and scaling behavior in human brain oscillations. J Neurosci Off J Soc Neurosci. 2001 Feb 15;21(4):1370–7.

8. He BJ. Scale-Free Properties of the Functional Magnetic Resonance Imaging Signal during Rest and Task. J Neurosci. 2011 Sep 28;31(39):13786–95.

9. Palva JM, Zhigalov A, Hirvonen J, Korhonen O, Linkenkaer-Hansen K, Palva S. Neuronal long-range temporal correlations and avalanche dynamics are correlated with behavioral scaling laws. Proc Natl Acad Sci. 2013 Feb 26;110(9):3585–90.

10. Zhigalov A, Arnulfo G, Nobili L, Palva S, Palva JM. Relationship of fast- and slow-timescale neuronal dynamics in human MEG and SEEG. J Neurosci Off J Soc Neurosci. 2015 Apr 1;35(13):5385–96.

11. Linkenkaer-Hansen K, Smit DJA, Barkil A, van Beijsterveldt TEM, Brussaard AB, Boomsma DI, et al. Genetic contributions to long-range temporal correlations in ongoing oscillations. J Neurosci Off J Soc Neurosci. 2007 Dec 12;27(50):13882–9.

12. Linkenkaer-Hansen K. Breakdown of Long-Range Temporal Correlations in Theta Oscillations in Patients with Major Depressive Disorder. J Neurosci. 2005 Nov 2;25(44):10131–7.

13. Montez T, Poil S-S, Jones BF, Manshanden I, Verbunt JPA, van Dijk BW, et al. Altered temporal correlations in parietal alpha and prefrontal theta oscillations in early-stage Alzheimer disease. Proc Natl Acad Sci. 2009 Feb 3;106(5):1614–9.

14. van Vreeswijk C, Sompolinsky H. Chaos in neuronal networks with balanced excitatory and inhibitory activity. Science. 1996 Dec 6;274(5293):1724–6.

15. Poil S-S, Hardstone R, Mansvelder HD, Linkenkaer-Hansen K. Critical-State Dynamics of Avalanches and Oscillations Jointly Emerge from Balanced Excitation/Inhibition in Neuronal Networks. J Neurosci. 2012 Jul 18;32(29):9817–23.

16. Deco G, Ponce-Alvarez A, Hagmann P, Romani GL, Mantini D, Corbetta M. How local excitation-inhibition ratio impacts the whole brain dynamics. J Neurosci Off J Soc Neurosci. 2014 Jun 4;34(23):7886–98.

17. Froemke RC. Plasticity of Cortical Excitatory-Inhibitory Balance. Annu Rev Neurosci. 2015 Jul 8;38(1):195–219.

18. Lam NH, Borduqui T, Hallak J, Roque AC, Anticevic A, Krystal JH, et al. Effects of Altered Excitation-Inhibition Balance on Decision Making in a Cortical Circuit Model. bioRxiv. 2017 Jan;

19. Wang X-J. Decision making in recurrent neuronal circuits. Neuron. 2008 Oct 23;60(2):215–34.

20. Eckhoff P, Wong-Lin KF, Holmes P. Optimality and Robustness of a Biophysical Decision-Making Model under Norepinephrine Modulation. J Neurosci. 2009 Apr 1;29(13):4301–11.

21. van Loon AM, Knapen T, Scholte HS, St. John-Saaltink E, Donner TH, Lamme VAF. GABA Shapes the Dynamics of Bistable Perception. Curr Biol. 2013 May;23(9):823–7.

22. Marder E. Neuromodulation of neuronal circuits: back to the future. Neuron. 2012 Oct 4;76(1):1–11.

23. Aston-Jones G, Cohen JD. An integrative theory of locus coeruleus-norepinephrine function: adaptive gain and optimal performance. Annu Rev Neurosci. 2005;28:403–50.

24. Berridge CW. Noradrenergic modulation of arousal. Brain Res Rev. 2008 Jun;58(1):1–17.

25. Harris KD, Thiele A. Cortical state and attention. Nat Rev Neurosci. 2011 Aug 10;12(9):509–23.

26. Lee S-H, Dan Y. Neuromodulation of brain states. Neuron. 2012 Oct 4;76(1):209–22.

27. Polack P-O, Friedman J, Golshani P. Cellular mechanisms of brain state-dependent gain modulation in visual cortex. Nat Neurosci. 2013 Sep;16(9):1331–9.

28. Fu Y, Tucciarone JM, Espinosa JS, Sheng N, Darcy DP, Nicoll RA, et al. A cortical circuit for gain control by behavioral state. Cell. 2014 Mar 13;156(6):1139–52.

29. Eggermann E, Kremer Y, Crochet S, Petersen CCH. Cholinergic Signals in Mouse Barrel Cortex during Active Whisker Sensing. Cell Rep. 2014 Dec;9(5):1654–60.

30. Chen N, Sugihara H, Sur M. An acetylcholine-activated microcircuit drives temporal dynamics of cortical activity. Nat Neurosci. 2015 Jun;18(6):892–902.

31. Moreno-Bote R, Rinzel J, Rubin N. Noise-induced alternations in an attractor network model of perceptual bistability. J Neurophysiol. 2007 Sep;98(3):1125–39.

32. Noest AJ, van Ee R, Nijs MM, van Wezel RJA. Percept-choice sequences driven by interrupted ambiguous stimuli: A low-level neural model. J Vis. 2007 Jun 21;7(8):10.

33. Crochet S, Poulet JFA, Kremer Y, Petersen CCH. Synaptic Mechanisms Underlying Sparse Coding of Active Touch. Neuron. 2011 Mar;69(6):1160–75.

34. Haider B, Häusser M, Carandini M. Inhibition dominates sensory responses in the awake cortex. Nature. 2013 Jan 3;493(7430):97–100.

35. Donner TH, Sagi D, Bonneh YS, Heeger DJ. Retinotopic Patterns of Correlated Fluctuations in Visual Cortex Reflect the Dynamics of Spontaneous Perceptual Suppression. J Neurosci. 2013 Jan 30;33(5):2188–98.

36. Brouwer GJ, van Ee R. Visual cortex allows prediction of perceptual states during ambiguous structure-from-motion. 2007;27(5):1015–23.

37. Beggs JM, Plenz D. Neuronal avalanches in neocortical circuits. J Neurosci Off J Soc Neurosci. 2003 Dec 3;23(35):11167–77.

38. Shew WL, Yang H, Petermann T, Roy R, Plenz D. Neuronal avalanches imply maximum dynamic range in cortical networks at criticality. J Neurosci Off J Soc Neurosci. 2009 Dec 9;29(49):15595–600.

39. Donner TH, Siegel M. A framework for local cortical oscillation patterns. Trends Cogn Sci. 2011 May;15(5):191–9.

40. Bauer M, Kluge C, Bach D, Bradbury D, Heinze HJ, Dolan RJ, et al. Cholinergic enhancement of visual attention and neural oscillations in the human brain. 2012;22(5):397–402.

41. Reimer J, Froudarakis E, Cadwell CR, Yatsenko D, Denfield GH, Tolias AS. Pupil fluctuations track fast switching of cortical states during quiet wakefulness. Neuron. 2014 Oct 22;84(2):355–62.

42. McGinley MJ, David SV, McCormick DA. Cortical Membrane Potential Signature of Optimal States for Sensory Signal Detection. Neuron. 2015 Jul 1;87(1):179–92.

43. Vinck M, Batista-Brito R, Knoblich U, Cardin JA. Arousal and locomotion make distinct contributions to cortical activity patterns and visual encoding. Neuron. 2015 May 6;86(3):740–54.

44. Meindertsma T, Kloosterman NA, Nolte G, Engel AK, Donner TH. Multiple Transient Signals in Human Visual Cortex Associated with an Elementary Decision. J Neurosci. 2017 May 11;3835–16.

45. Murphy PR, G O Redmond, Michael O, Robertson IH, Balsters JH. Pupil diameter covaries with BOLD activity in human locus coeruleus. Hum Brain Mapp. 2014;35(8):4140–54.

46. Joshi S, Li Y, Kalwani RM, Gold JI. Relationships between Pupil Diameter and Neuronal Activity in the Locus Coeruleus, Colliculi, and Cingulate Cortex. Neuron. 2016 Jan 6;89(1):221–34.

47. Reimer J, McGinley MJ, Liu Y, Rodenkirch C, Wang Q, McCormick DA, et al. Pupil fluctuations track rapid changes in adrenergic and cholinergic activity in cortex. Nat Commun. 2016 Nov 8;7:13289.

48. de Gee JW, Colizoli O, Kloosterman NA, Knapen T, Nieuwenhuis S, Donner TH. Dynamic modulation of decision biases by brainstem arousal systems. eLife [Internet]. 2017 Apr 11 [cited 2017 May 16];6. Available from: http://elifesciences.org/lookup/doi/10.7554/eLife.23232

49. Denève S, Machens CK. Efficient codes and balanced networks. Nat Neurosci. 2016 Feb 23;19(3):375–82.

50. Yizhar O, Fenno LE, Prigge M, Schneider F, Davidson TJ, O'Shea DJ, et al. Neocortical excitation/inhibition balance in information processing and social dysfunction. Nature. 2011 Jul 27;477(7363):171–8.

51. Lisman J. Excitation, inhibition, local oscillations, or large-scale loops: what causes the symptoms of schizophrenia? Curr Opin Neurobiol. 2012 Jun;22(3):537–44.

52. Nelson SB, Valakh V. Excitatory/Inhibitory Balance and Circuit Homeostasis in Autism Spectrum Disorders. Neuron. 2015 Aug 19;87(4):684–98.

53. Fuchs T, Jefferson SJ, Hooper A, Yee P-H, Maguire J, Luscher B. Disinhibition of somatostatin-positive GABAergic interneurons results in an anxiolytic and antidepressant-like brain state. Mol Psychiatry. 2017 Jun;22(6):920–30.

54. Isaacson JS, Scanziani M. How inhibition shapes cortical activity. Neuron. 2011 Oct 20;72(2):231–43.

55. Froemke RC, Merzenich MM, Schreiner CE. A synaptic memory trace for cortical receptive field plasticity. Nature. 2007 Nov 15;450(7168):425–9.

56. Martins ARO, Froemke RC. Coordinated forms of noradrenergic plasticity in the locus coeruleus and primary auditory cortex. Nat Neurosci. 2015 Aug 24;18(10):1483–92.

57. Sara SJ. The locus coeruleus and noradrenergic modulation of cognition. Nat Rev Neurosci. 2009 Mar;10(3):211–23.

58. Dayan P. Twenty-Five Lessons from Computational Neuromodulation. Neuron. 2012 Oct;76(1):240–56.

59. Robbins TW, Arnsten AFT. The neuropsychopharmacology of fronto-executive function: monoaminergic modulation. Annu Rev Neurosci. 2009;32:267–87.

60. Montague PR, Hyman SE, Cohen JD. Computational roles for dopamine in behavioural control. Nature. 2004 Oct 14;431(7010):760–7.

61. Haber SN, Knutson B. The reward circuit: linking primate anatomy and human imaging. Neuropsychopharmacol Off Publ Am Coll Neuropsychopharmacol. 2010 Jan;35(1):4–26.

62. Morrison JH, Foote SL. Noradrenergic and serotoninergic innervation of cortical, thalamic, and tectal visual structures in Old and New World monkeys. J Comp Neurol. 1986 Jan 1;243(1):117–38.

63. Ramos BP, Arnsten AFT. Adrenergic pharmacology and cognition: focus on the prefrontal cortex. Pharmacol Ther. 2007 Mar;113(3):523–36.

64. Salgado H, Treviño M, Atzori M. Layer- and area-specific actions of norepinephrine on cortical synaptic transmission. Brain Res. 2016 Jun 15;1641(Pt B):163–76.

65. Pfeffer CK, Xue M, He M, Huang Z, Scanziani M. Inhibition of inhibition in visual cortex: the logic of connections between molecularly distinct interneurons. Nat Neurosci. 2013;16(8):1068–76.

66. Pakan JM, Lowe SC, Dylda E, Keemink SW, Currie SP, Coutts CA, et al. Behavioral-state modulation of inhibition is context-dependent and cell type specific in mouse visual cortex. Elife. 2016;5.

67. Linkenkaer-Hansen K, Nikulin VV, Palva S, Ilmoniemi RJ, Palva JM. Prestimulus oscillations enhance psychophysical performance in humans. J Neurosci Off J Soc Neurosci. 2004 Nov 10;24(45):10186–90.

68. Swadlow HA. Thalamocortical control of feed-forward inhibition in awake somatosensory “barrel” cortex. Philos Trans R Soc B Biol Sci. 2002 Dec 29;357(1428):1717–27.

69. Kepecs A, Fishell G. Interneuron cell types are fit to function. Nature. 2014 Jan 15;505(7483):318–26.

70. Ponce-Alvarez A, He BJ, Hagmann P, Deco G. Task-Driven Activity Reduces the Cortical Activity Space of the Brain: Experiment and Whole-Brain Modeling. Graham LJ, editor. PLOS Comput Biol. 2015 Aug 28;11(8):e1004445.

71. Carter OL, Pettigrew JD, Hasler F, Wallis GM, Liu GB, Hell D, et al. Modulating the rate and rhythmicity of perceptual rivalry alternations with the mixed 5-HT2A and 5-HT1A agonist psilocybin. Neuropsychopharmacol Off Publ Am Coll Neuropsychopharmacol. 2005 Jun;30(6):1154–62.

72. Noudoost B, Moore T. Control of visual cortical signals by prefrontal dopamine. Nature. 2011 May 15;474(7351):372–5.

73. Honey CJ, Thesen T, Donner TH, Silbert LJ, Carlson CE, Devinsky O, et al. Slow Cortical Dynamics and the Accumulation of Information over Long Timescales. Neuron. 2012 Oct;76(2):423–34.

74. Murray JD, Bernacchia A, Freedman DJ, Romo R, Wallis JD, Cai X, et al. A hierarchy of intrinsic timescales across primate cortex. Nat Neurosci. 2014 Nov 10;17(12):1661–3.

75. Chaudhuri R, Knoblauch K, Gariel M-A, Kennedy H, Wang X-J. A Large-Scale Circuit Mechanism for Hierarchical Dynamical Processing in the Primate Cortex. Neuron. 2015 Oct 21;88(2):419–31.

76. Wang X-JJ. Probabilistic decision making by slow reverberation in cortical circuits. 2002;36(5):955–68.

77. Beggs JM. The criticality hypothesis: how local cortical networks might optimize information processing. Philos Transact A Math Phys Eng Sci. 2008 Feb 13;366(1864):329–43.

78. Bak P, Tang C, Wiesenfeld K. Self-organized criticality: An explanation of the 1/f noise. Phys Rev Lett. 1987 Jul 27;59(4):381–4.

79. Bak P. How nature works: the science of self-organized criticality [Internet]. New York, NY, USA: Copernicus; 1996 [cited 2017 Apr 20]. Available from: http://catalog.hathitrust.org/api/volumes/oclc/34623628.html

80. Chialvo DR. Emergent complex neural dynamics. Nat Phys. 2010 Oct;6(10):744–50.

81. Hesse J, Gross T. Self-organized criticality as a fundamental property of neural systems. Front Syst Neurosci. 2014;8:166.

82. Kinouchi O, Copelli M. Optimal dynamical range of excitable networks at criticality. Nat Phys. 2006 May;2(5):348–51.

83. Shew W, Yang H, Yu S, Roy R. Information capacity and transmission are maximized in balanced cortical networks with neuronal avalanches. J …. 2011;

84. Shriki O, Yellin D. Optimal Information Representation and Criticality in an Adaptive Sensory Recurrent Neuronal Network. PLoS Comput Biol. 2016 Feb;12(2):e1004698.

85. Priesemann V, Valderrama M, Wibral M, Le Van Quyen M. Neuronal avalanches differ from wakefulness to deep sleep--evidence from intracranial depth recordings in humans. PLoS Comput Biol. 2013;9(3):e1002985.

86. Arviv O, Goldstein A, Shriki O. Near-Critical Dynamics in Stimulus-Evoked Activity of the Human Brain and Its Relation to Spontaneous Resting-State Activity. J Neurosci Off J Soc Neurosci. 2015 Oct 14;35(41):13927–42.

87. Fagerholm ED, Lorenz R, Scott G, Dinov M, Hellyer PJ, Mirzaei N, et al. Cascades and Cognitive State: Focused Attention Incurs Subcritical Dynamics. J Neurosci. 2015 Mar 18;35(11):4626–34.

88. Shew WL, Clawson WP, Pobst J, Karimipanah Y, Wright NC, Wessel R. Adaptation to sensory input tunes visual cortex to criticality. Nat Phys. 2015 Jun 22;11(8):659–63.

89. Tiseo, Rogers, Friedhoff. Pharmacokinetic and pharmacodynamic profile of donepezil HCl following evening administration: Evening administration of donepezil HCl. Br J Clin Pharmacol. 1998 Jan 4;46(S1):13–8.

90. Sauer J-M, Ring BJ, Witcher JW. Clinical pharmacokinetics of atomoxetine. Clin Pharmacokinet. 2005;44(6):571–90.

91. Wallach H, O'connell DN. The kinetic depth effect. J Exp Psychol. 1953 Apr;45(4):205–17.

92. Sperling G, Dosher BA, Landy MS. How to study the kinetic depth effect experimentally. J Exp Psychol Hum Percept Perform. 1990 May;16(2):445–50.

93. Engbert R, Kliegl R. Microsaccades uncover the orientation of covert attention. Vision Res. 2003 Apr;43(9):1035–45.

94. Oostenveld R, Fries P, Maris E, Schoffelen J-M. FieldTrip: Open source software for advanced analysis of MEG, EEG, and invasive electrophysiological data. Comput Intell Neurosci. 2011;2011:156869.

95. Bell AJ, Sejnowski TJ. An information-maximization approach to blind separation and blind deconvolution. Neural Comput. 1995 Nov;7(6):1129–59.

96. Hyvarinen A. Fast and robust fixed-point algorithms for independent component analysis. IEEE Trans Neural Netw. 1999 May;10(3):626–34.

97. Hipp JF, Siegel M. Dissociating neuronal gamma-band activity from cranial and ocular muscle activity in EEG. Front Hum Neurosci [Internet]. 2013 [cited 2017 Apr 20];7. Available from: http://journal.frontiersin.org/article/10.3389/fnhum.2013.00338/abstract

98. Mitra PP, Pesaran B. Analysis of dynamic brain imaging data. Biophys J. 1999 Feb;76(2):691–708.

99. Pascual-Marqui RD, Lehmann D, Koukkou M, Kochi K, Anderer P, Saletu B, et al. Assessing interactions in the brain with exact low-resolution electromagnetic tomography. Philos Transact A Math Phys Eng Sci. 2011 Oct 13;369(1952):3768–84.

100. Nolte G. The magnetic lead field theorem in the quasi-static approximation and its use for magnetoencephalography forward calculation in realistic volume conductors. Phys Med Biol. 2003 Nov 21;48(22):3637–52.

101. Pfeffer T, Linkenkaer-Hansen K, Avramiea A-E, Engel AK, Donner TH. Noradrenaline increases long-range temporal correlations of neuronal alpha oscillations in the human cortex. In 2015. p. 393.27.

102. Peng CK, Buldyrev SV, Havlin S, Simons M, Stanley HE, Goldberger AL. Mosaic organization of DNA nucleotides. Phys Rev E Stat Phys Plasmas Fluids Relat Interdiscip Top. 1994 Feb;49(2):1685–9.

103. Hardstone R, Poil S-S, Schiavone G, Jansen R, Nikulin VV, Mansvelder HD, et al. Detrended Fluctuation Analysis: A Scale-Free View on Neuronal Oscillations. Front Physiol [Internet]. 2012 [cited 2017 Apr 20];3. Available from: http://journal.frontiersin.org/article/10.3389/fphys.2012.00450/abstract

104. Rouder JN, Speckman PL, Sun D, Morey RD, Iverson G. Bayesian t tests for accepting and rejecting the null hypothesis. Psychon Bull Rev. 2009 Apr;16(2):225–37.

105. Wetzels R, Wagenmakers E-J. A default Bayesian hypothesis test for correlations and partial correlations. Psychon Bull Rev. 2012 Dec;19(6):1057–64.

106. Nichols TE, Holmes AP. Nonparametric permutation tests for functional neuroimaging: A primer with examples. Hum Brain Mapp. 2002 Jan;15(1):1–25.

107. Maris E, Oostenveld R. Nonparametric statistical testing of EEG- and MEG-data. J Neurosci Methods. 2007 Aug 15;164(1):177–90.

108. Eiben AE, Smit SK. Parameter tuning for configuring and analyzing evolutionary algorithms. Swarm Evol Comput. 2011 Mar;1(1):19–31.

109. Goodman DF, Stimberg M, Yger P, Brette R. Brian 2: neural simulations on a variety of computational hardware. BMC Neurosci. 2014;15(Suppl 1):P199.

SUPPLEMENTARY FIGURES

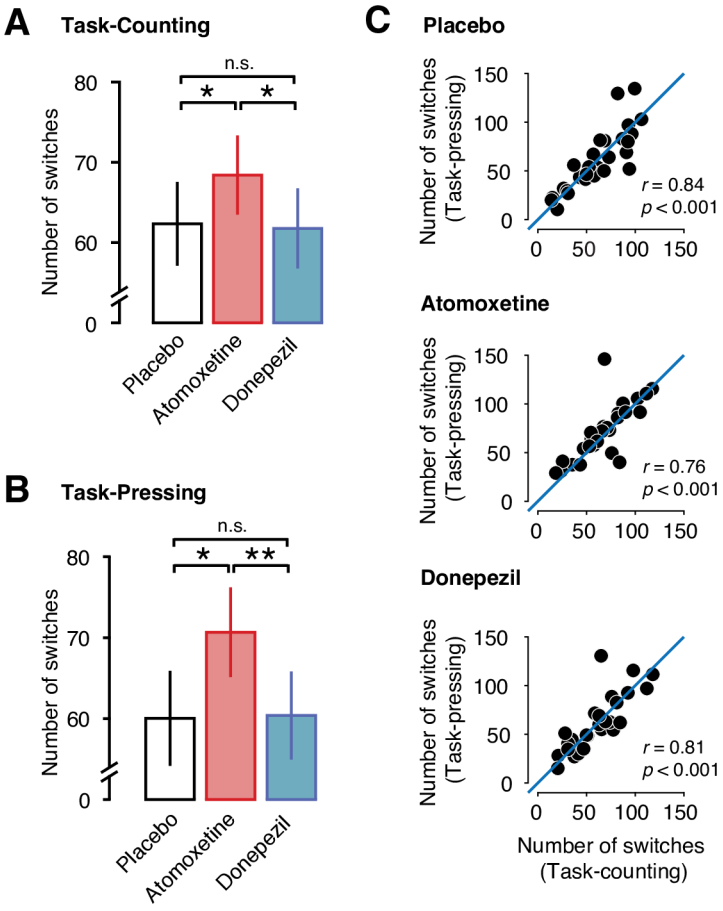

S1 Fig. Similar atomoxetine-related effects in both Task-counting and Task-resting conditions. **(A)** Number of perceptual alternations reported by the subjects per 10 min run for Task-counting condition. **(B)** Same as (A), but for Task-pressing condition. **(C)** Relation between the number of reported alternations during Task-counting (x-axis) and Task-pressing (y-axis). The blue line depicts a linear relation with slope 1 as a reference.

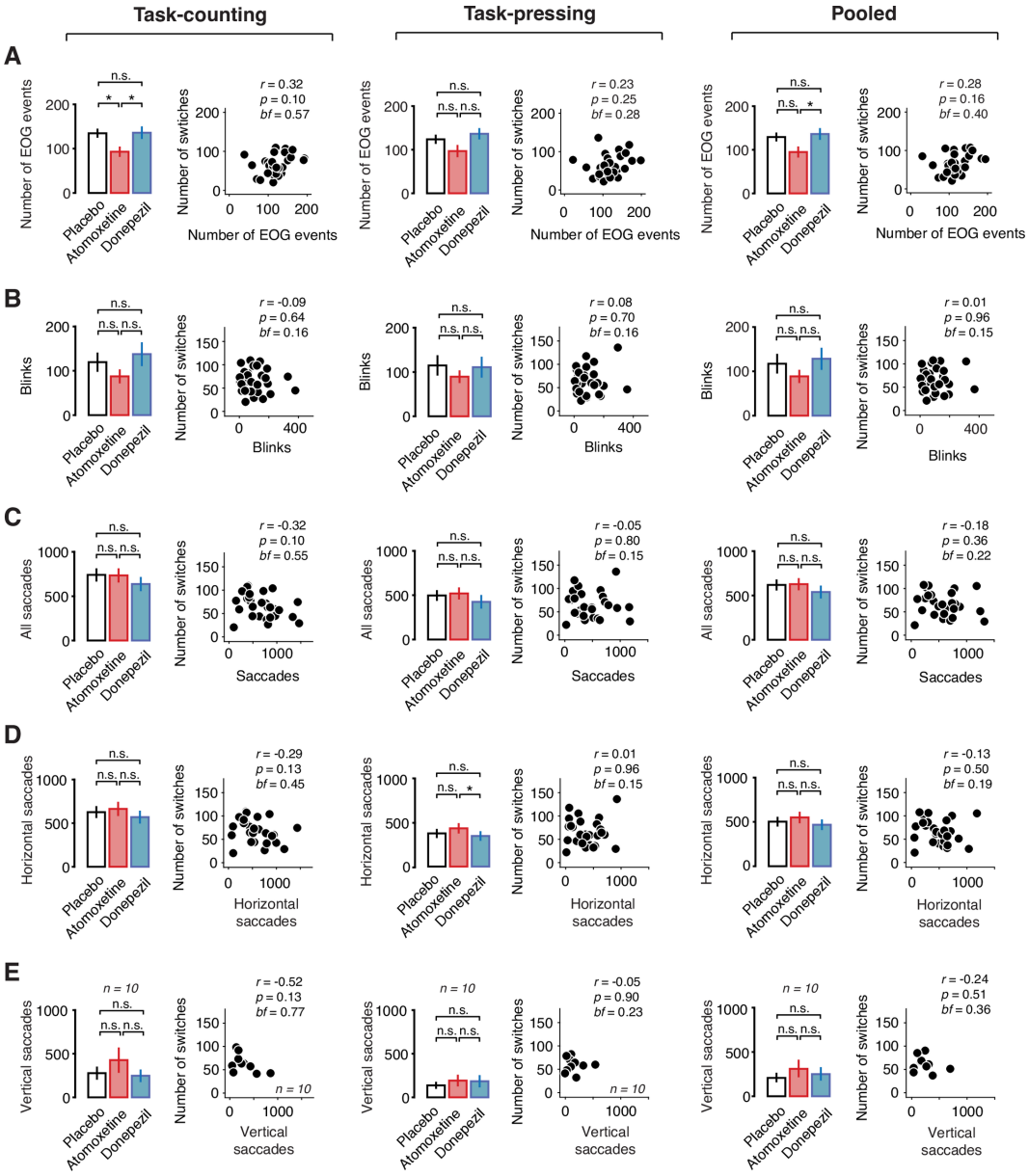

S2 Fig. Change in perceptual alternation rate is not due to change in blinks or fixational eye movements. **(A)** Number of EOG events for during Task-counting (left), Task-pressing (middle) and pooled across both conditions (right). Scatter plots depict the relation between the number of EOG events (x-axis) and the number of reported perceptual alternations (y-axis). **(B)** Same as (A), but for the number of detected eye blinks. **(C)** Same as (A) and (B), but for the number of saccades (horizontal and vertical). **(D)** Same as (C), but for horizontal saccades only. **(E)** Same as (D), but for vertical saccades only.

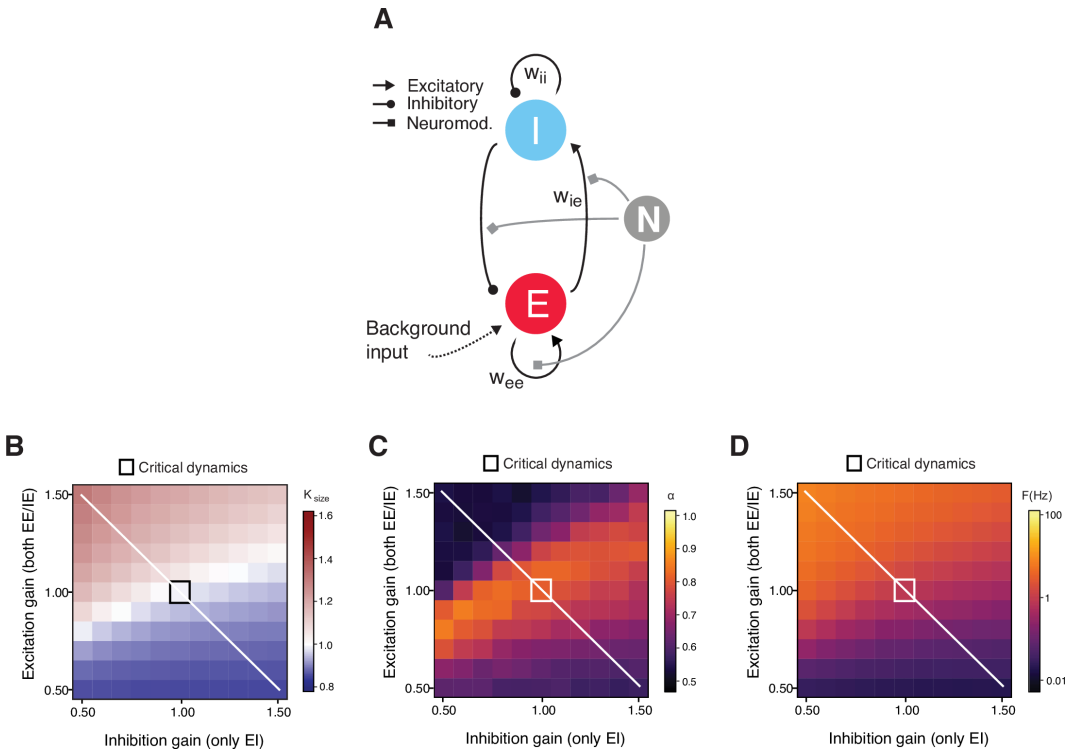

S3 Fig. Different version of modulation of E/I ratio in cortical patch model **(A)** Neuromodulation was simulated as a gain modulation term multiplied with excitatory (EE and IE) and/or inhibitory (EI only) synaptic weights. **(B)** κ as a function of excitatory and inhibitory connectivity (with a spacing of 2.5%; means across 10 simulations per cell). The region of $\kappa \sim 1$, overlaps with the region of $\alpha > 0.5$ and splits the phase space into an excitation-dominant ($\kappa > 1$) and an inhibition-dominant region ($\kappa < 1$). **(C)** Same as (B), but for scaling exponent α. **(D)** Same as (B) and (C), but for firing rate.

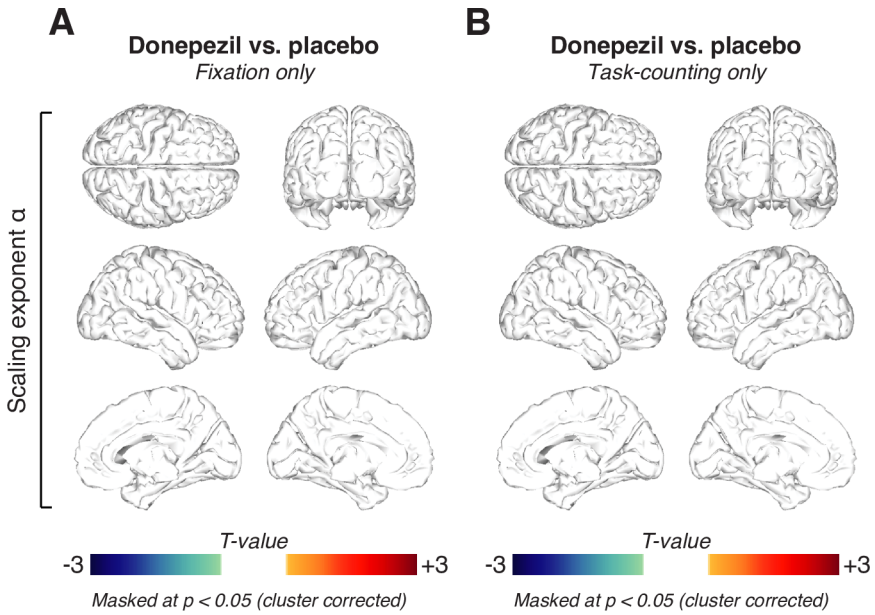

S4 Fig. No donepezil-related changes in scaling exponent in neither behavioral contexts. **(A)** Spatial distribution of donepezil-induced changes in scaling exponent α during Fixation, thresholded at p = 0.05 (two-sided cluster-based permutation test). **(B)** As (A), but for Task-counting.